Dihydroartemisinin Shows Promising Effects in the Treatment of Experimental Autoimmune Encephalomyelitis and Maintains Inflammatory Homeostasis by Targeting AXL in Microglia

Zhu Xiaoxin (zhuxx@icmm.ac.cn)
China Academy of Chinese Medical Sciences Institute of Chinese Materia Medica
https://orcid.org/0000-0003-2948-3395

Ran Qingsen
China Academy of Chinese Medical Sciences Institute of Chinese Materia Medica

Qi Li
China Academy of Chinese Medical Sciences Institute of Chinese Materia Medica

Liu Li
China Academy of Chinese Medical Sciences Institute of Chinese Materia Medica

Sun Lidong
China Academy of Chinese Medical Sciences

Yang Qing
China Academy of Chinese Medical Sciences

Li Yujie
China Academy of Chinese Medical Sciences

Chen Ying
China Academy of Chinese Medical Sciences

Weng Xiaogang
China Academy of Chinese Medical Sciences

Wang Yajie
China Academy of Traditional Chinese Medicine: China Academy of Chinese Medical Sciences

Cai Weiyan
China Academy of Chinese Medical Sciences

Research article

Keywords: Dihydroartemisinin, EAE, AXL, Microglia, Inflammation homeostasis, Multiple Sclerosis

Posted Date: December 10th, 2020

DOI: https://doi.org/10.21203/rs.3.rs-122856/v1

Abstract

Background: During EAE progression, the endogenous mechanisms mediating nervous autoimmune inflammation balance, as represented by AXL, were proved to be pathologically disturbed, immune balance and axon repair. Therapeutically, by activating AXL signaling, the inflammatory rebalance from promotion to resolution has attracted increasing attention and showed advantages in autoimmune disease treatment. Previous studies implied that DHA had potential effects in treating autoimmune diseases. However, the detailed mechanisms in inflammation regulation, especially in CNS, remain unclear.

Methods: C57BL/6 mice were immunized with MOG_{35-55} and treated daily with DHA. Then clinical scores, pathology, and ethology features of EAE were assessed through histological staining (H&E, LFB staining), TEM and gait analysis. Moreover, DHA-responsive cells and genes were screened by 10x Genomics. The immunological responses to DHA were measured by flow cytometry and fluorescence microscope in BV2 cells. The concentrations and bio-activities of chemokines were respectively evaluated through ELISA and trans-well assay.

Results: After DHA treatment, the clinical scores and body weight were significantly improved. Histologically, mice showed slighter spinal cord lesion, less inflammatory cuffs. By using gait analysis, DHA obviously improved physical coordination. 10x Genomics demonstrated that DHA selectively upregulated AXL expression in microglia. Immunologically, by enhancing AXL signaling, the phagocytic and chemotactic potential of microglia and the Treg differentiation followed by upregulating PDL1 were significantly influenced by DHA. Conversely, specific blocking of AXL by SGI7079 was sufficient to reverse above-mentioned functions. Molecularly, DHA specifically rebalanced the overactivated inflammation through STAT1:SOCS3: AXL: IFNAR pathway.

Conclusions: The present study highlighted the central role of AXL signaling in DHA mediated inflammatory transition.

Background

Featuring the unresolved inflammation in central nervous system (CNS) and persistent demyelination, multiple sclerosis(MS) is the most prevalent and, to date, incurable chronic autoimmune disease, which inflicts more than 2 million people worldwide[1]. Sharing the similar pathological features and progression pattern with MS, EAE is the most widely-used mouse model for the research and development of anti-MS drugs[2].

Therapeutically, as represented by methylprednisolone, the exogenous suppression of inflammation was chosen as the limited strategy and widely applied for MS treatments, leaving severe side-effects[3]. Hopefully, leading by the inflammation transition and balancing theory, candidates capable of mediating inflammation resolution have attracted increasing attention in recent autoimmune disease treatment. Microglia, resident CNS immune cells of monocyte lineage, participate in both exacerbating and resolving

CNS inflammation upon any perturbations[4, 5]. Specifically, the aberrant activated microglia play a core role in the induction of EAE or MS by secreting a battery of proinflammatory cytokines and unbalanced autoantigen presentation. In contrast, it also exhibits regenerative properties through phagocytizing myelin debris and secreting growth and neurotrophic factors[6–8]. Hence, the functional regulation of the dynamic properties of microglia may deeply influenced the transition and balance of autoimmune inflammation and further provide a therapeutic protection to CNS injury.

Recent studies revealed the complexity of autoinflammatory network integrated multiple physio-pathological procedures. Among them, Chemoattraction, uptake and presentation of myelin debris were proved to be the central events tightly correlating to the treatment and prognosis for MS patients[9, 10]. Firstly, Chemoattraction procedures, mainly dominated by CCL5 and their receptor CCR5 in EAE, have proved to play crucial roles in the trafficking of encephalitogenic T cells and consequently leading to demyelination [11, 12]. Secondly, in response to danger signals or autoantigens carried by resident tissue debris, Treg functions as a main braker for auto-neuroinflammation. Further studies revealed that, as the negative co-regulatory molecule, PDL1 provided the indispensable differentiational signals from CD4 + T cell to Treg [13, 14]. Most importantly, disruption of costimulatory signals or augmentation of coinhibitory ones are therapeutically considered to be an attractive approach for Treg-mediated self-limitation of inflammation, which makes it a promising strategy in EAE therapy[15].

Mechanistically, AXL, one of the TAM family of receptor tyrosine kinases, referred to play pivotal roles in regulating myelination, inflammation and phagocytosis in the nervous system whereby it widely defines multiple features for microglial physiology[16, 17]. Interestingly, by sensing and mediating the inflammatory signaling from TLRs, the IFNAR:STAT1 signaling can efficiently induce the activation of TAMs, which in turn usurps the pro-inflammatory signals dominated IFNAR:STAT1 cascade and simultaneously upregulates the expression of inflammation suppressors, SOCS1 and SOCS3. Within this negative feedback loop, the AXL:IFNAR:STAT1 pathway forms the most fundamental endogenous mechanism for inflammation balance and transition from promotion to resolution, contributing to inflammation self-restriction and protection to autoimmune damages[18, 19]. The failure of this mechanism has been systematically revealed in MS diseases progression. Therapeutically, up-regulation of AXL in MS lesions was proved to be beneficial for: (1) the blockage of the inappropriate activation of the immune response, (2) the protection of resident CNS cells against apoptosis and (3) the clearance of myelin debris [20–22].

Artemisinin, a sesquiterpene lactone isolated from the Chinese herbal medicine *Artemisia annua L*., was identified by Tu Youyou who has been awarded for Nobel Prize in 2015 [23]. It is famous for anti-malaria effect. DHA is an active metabolite shared by all artemisinin compounds (artemisinin, artesunate, artemether, and so on) and shows more potency against malaria than other artemisinin compounds [24]. Apart from its prominent anti-malaria effect, DHA is involved in a spectrum of cellular functions, including tumor cell growth, angiogenesis, and immune regulation. In addition, DHA is initially demonstrated as an effective treatment option for SLE and currently being assessed in a Chinese clinical trial [25]. Moreover, it was also proved to possess efficacy against a wide arrange of autoimmune diseases depending on its

limited influence on T cells.[26]. However, the detailed mechanisms of DHA in inflammation resolution, especially in MS, remain poorly understood.

In our study, in EAE, we investigated whether AXL acts as a therapeutic target in switching of inflammation transition to protect CNS against inflammatory injury. Pharmacologically, by enhancing AXL signaling through STAT1:SOCS3 pathway in microglia, we detected how DHA regulates CNS inflammation from promotion to inhibition.

Materials And Methods

Animal experiment and Reagents

Female C57BL/6 mice were obtained from institute of basic theory of Chinese medicine, China academy of Chinese medicine, and were used at 8 to 10 weeks of age. All mice were housed under specific pathogen-free conditions. All experiments were performed according to the institutional ethical guidelines on animal care and approved by the Institute Animal Care and Use Committee at Beijing Institute of Materia Medica. SGI7079(MCE; HY-12964); Human IFN-β (300-02BC-20); Fludarabine (MCE; B-0069); Mouse CCL5 ELISA kit (Proteintech, KE10017).

Induction, treatment, and clinical evaluation of EAE

C57BL/6 mice were immunized with MOG_{35-55} ($3^{mg.ml-1}$; Celtek Bioscience, Franklin, TN) emulsified in an equal volume of CFA composed of mycobacterium tuberculosis H37RA (10 $mg.ml^{-1}$; Difco Laboratories, Detroit, MI) in Complete Freund's Adjuvant (Sigma-Aldrich). Mice were anaesthetized with isoflurane and 120 µl of emulsion was injected subcutaneously on each flank (200 µl total/mouse) on day 0. In addition, 500 µl of pertussis toxin (1$µg.ml^{-1}$; List Biological Laboratories, Campbell, CA) was injected into the tail vein on days 0 and 2. DHA (Chongqing Holley Wuling Mountain Pharmaceutical Company, purity≥99%; 2, 10 or 20 $mg.kg^{-1}$) and Methylprednisolone (Pfizer; 1$mg.kg^{-1}$) were suspended in 0.5% (w/v) carboxymethylcellulose solution and orally administered via gavage once daily. Clinical assessment of EAE was performed daily and mice were scored for disease according to the following criteria: 0, no overt signs of disease; 1, limp tail or hind limb weakness but not both; 2, limp tail and hind limb weakness; 3, partial hind limb paralysis; 4, complete hind limb paralysis; 5, moribund state or dead.

Cell Culture

All cells were maintained in culture medium supplemented with 10% fetal bovine serum (Gibco, USA) at 37 °C in a humidified incubator (5% CO2) (SANYO, JAPAN), with Jurkat T cells in RPMI-1640 medium and PC12 cells and BV 2 cells in DMEM medium.

Histopathology

To assess the degree of CNS inflammation and demyelination, C57BL/6 mice treated with vehicle or DHA were anesthetized by pentobarbital sodium and perfused by intracardiac injection of PBS containing 4% paraformaldehyde. Paraffin embedded 5 mm sections of spinal cord were stained with H&E and Luxol Fast Blue (LFB) and then examined by light microscopy. Lumbar spinal cords were sliced into 1mm sections. Tin sections were cut, stained with uranyl acetate and lead citrate and then analyzed under transmission electron microscope (Olympus, JAPAN) . Briefly, inflammation was scored as follows: 0, none; 1, a few inflammatory cells; 2, organization of perivascular infiltrates; 3, increasing severity of perivascular cuffing with extension into adjacent tissue. Demyelination was scored as follows: 0, none; 1, rare foci; 2, a few areas of demyelination; 3, large (confluent) areas of demyelination.

Gait analysis

Gait assessment was carried out as described previously[27]. on the 24th day when the EAE mice were at the peak period by the automated computer-assisted method (Xin Hai Hua Yi Instrument Co., Beijing China). Data were collected and analyzed with Gait Analysis Lab software version 5.0. The equipment was located under natural light in a silent room. In brief, the system consists of an elevated 1.2 m-long glass plate which is illuminated with a fluorescent light coming from the side and the fluorescent light is internally reflected in the glass allowing the paws to reflect light as they come into contact with the glass floor. A ceiling on top of the walkway creates a red background to produce the contour of the animal. A high-speed camera (100 frames) underneath the glass plate captures the images which are subsequently analyzed by the connected computer program. The video acquisition system is sealed with a PVC sheet to ensure a uniform dark environment to insure controlled lighting in the experiment. Prior to the first testing day, the animals were trained to traverse a glass walkway toward their home cage. On subsequent training days, three complete runs across the walkway were recorded by a camera positioned below. If an animal failed to complete a run within 5 s, walked backwards, or reared during the run, the animal was given an additional re-run. Pixels below a light intensity of 20 units on a 0–255 arbitrary scale were filtered out. Prints can be inspected individually and in combinations, and timing diagrams for paw placements are available.

Isolation of mononuclear cell infiltrated in spinal cord

Spinal cord infiltrated mononuclear cells were isolated as described previously. The mice were anaesthetized with pentobarbital sodium and perfused with 20 ml of cold PBS. The spinal cords were extruded by flushing the vertebral canal with PBS and rinsed in PBS. Tissues were forced through 70 mM nylon cell strainers (BD Falcon), and then the spinal cord cell suspensions were incubated with collagenase IV (2 $mg.ml^{-1}$) and DNaseI (100$\mu g.ml^{-1}$) at 37℃ for 30 min, and passed again through 70 mM nylon cell strainers to yield single-cell suspensions. CNS mononuclear cells were centrifuged (500g)

at room temperature for 20 min over discontinuous 30%/ 70% Percoll gradient (GE Healthcare). Then, lysed by TRIzol Reagent (Invitrogen) for qRT-PCR analyze and loading buffer for western blot analyze.

Phagocytosis assay

Phagocytosis assays was assessed as described previously[28], PC12 cells were induced to an apoptotic state by serum deprivation for 48 hours after being cultured. BV2 cells were plated at a cell density of 2×10^5 cells. After induction of apoptosis, PC12 cells were harvested, stained with carboxy fluorescein diacetate succinimide ester (CFSE) and placed in contact with treated BV2 cells at a 3/1 ratio for 2 hours so phagocytosis would occur. After coculturing, the supernatant was removed, and BV2 cells were harvested and stained with anti-F4/80-PE conjugated anti-mouse antibody diluted in PBS (1/200) for 30 minutes at 4℃. After the incubation period, the cells taken to an flow cytometer and a total of 10 000 events were acquired. Double-stained events were considered as phagocytosing BV2 cells, and percentage of such events was used to quantify phagocytosis. Then used the fluorescence microscope for qualitative phagocytosis analysis.

Sample preparation for sequencing

The brain and spinal cords were extruded by flushing the vertebral canal with PBS and rinsed in PBS. Tissues were forced through 40 mM nylon cell strainers (BD Falcon), and then the spinal cord cell suspensions were incubated with collagenase (1 $mg.ml^{-1}$) DNaseI (100$\mu g.ml^{-1}$) at 37℃ for 60 min, and passed again through 40 mM nylon cell strainers to yield single-cell suspensions. To ensure the cell viability more than 90% by using the trypan blue.

10x Genomics single cell sequence

The single cell sequencing was assessed as described previously[29] and implemented by oebiotech. Cells were processed using the 10x Genomics Chromium Controller and the Chromium Single Cell 5' Library & Gel Bead Kit (PN 1000006) following the standard manufacturer's protocols (https://tinyurl.com/y96l7lns). Three technical replicates were run in parallel for each sample. In brief, between 14,000 and 21,000 live cells were loaded onto the Chromium controller in an effort to recover between 10,000 and 15,000 cells for library preparation and sequencing. Gel beads were prepared according to standard manufacturer's protocols. Oil partitions of single-cell + oligo coated gel beads (GEMs) were captured and reverse transcription was performed, resulting in cDNA tagged with a cell barcode and unique molecular index. Next, GEMs were broken and cDNA was amplified and quantified using an Agilent Bioanalyzer High Sensitivity chip (Agilent Technologies).

Real-time PCR Assay

Total RNA was isolated using Trizol reagent (Invitrogen), reverse transcribed, and polymerase chain reaction amplified using specific primers. three-Step Real-time PCR was performed with SYBR Green PCR Reagents (CWbio, China) was used with a total of 100 ng of RNA per reaction with PDL1, AXL, GAS6, RANTES, and ACTB (sequence was shown in supplementary data 1) primers according to the manufacturer's instructions. All results were normalized to ACTB as an internal control. The reactions were aliquoted in triplicate in an optical 96 well plate; RNase-free water was used as a blank. Reactions were run in the LightCycler 480 Ⅱ, USA real-time PCR machine (Roche) with the following cycles: 95°C for 10 min to activate the DNA polymerase, followed by 45 cycles at 53°C for 15 seconds, and 72°C for 1 min. The real-time quantification was monitored directly by the StepOnePlus software and the comparative thresholds were identified for each gene with each RNA sample and calculated at the end of the measurements. After normalization of the, the fold change was determined as fold change = $2^{-(\Delta\Delta CT)}$ where ΔΔCT is defined as the normalized change in CT between two groups. Statistics were performed on the normalized CT values. Premier Sequence: ACTB (Mus sapiens): Forward-5'-GGCTGTATTCCCCTCCATCG3'; Reverse-5'-CCAGTTGGTAACAATGCCATGT-3'. AXL (Mus sapiens): Forward-5'-GGAACCCGTGACCCTACT-3'; Reverse-5'-GACTCCCTTGGCATTGTG-3'. GAS6 (Mus sapiens): Forward-5'-TACAGGCTCAACTACACCCG-3'; Reverse-5'-ACTGCCAGGACCACCAAC-3'. CCL5 (Mus sapiens): Forward-5'-ACCACTCCCTGCTGCTTT-3'; Reverse-5'-ACACTTGGCGGTTCCTTC-3'. PDL1 (Mus sapiens): Forward-5'-GTGGTGCGGACTACAAGC-3'; Reverse-5'-CAGGCAGTTCTGGGATGA-3', CD80(Mus sapiens): Forward-5'-ATCCATCGGACTACATCG-3'; Reverse-5'-TAGGTAGTTCTGGGAAGC-3' .

Protein extraction and Western Blot analysis

BV2 cells were lysed using lysis buffer containing protease inhibitor phenylmethylsulfonyl fluoride (PMSF). Protein concentrations were measured using a bicinchoninic acid assay kit. Total sample was separated by 10 % sodium dodecyl sulfate-polyacrylamide gel electrophoresis (SDS-PAGE) and then blotted to polyvinylidene fluoride (PVDF) membranes (Merck Millipore, IPVH00010). Membranes were blocked for 2 h at room temperature with 5 % bovine serum albumin (BSA). Next, incubate with primary antibodies overnight at 4°C. Horseradish peroxidase-conjugated antibodies against mouse and rabbit were used as secondary antibodies. After extensive washing, blots were developed with an enhanced chemiluminescent plus assay kit (Thermo Scientific), developed on X-ray film, and analyzed by Image J software (National Institutes of Health, Bethesda, MD, USA).

Flow cytometry

For cell surface staining, cells first blocked with 3% FBS for 15 min in room temperature and then were stained with antibodies anti-PDL1-FITC (Proteintec, USA) for 1h 4 ℃ to analyze whether DHA influence the PDL1 expression on microglia and macrophages. For intracellular staining, cells were first used Triton-100 for 15 min in room temperature, and then used anti-FOXP3-FITC (Proteintec, USA) for 1 h 4 ℃ to

analyze whether DHA promote T cell differentiation into Treg cells. Finally, all cells were sorted on the BECKMAN Flow Cytometer.

Trans-well assay

A trans-well (8μm pore size; Falcon, USA) assay was used to further analyze chemotaxis ability of BV2 cells according to the manufacturer's instructions. BV2 cells at the density of 5×10^4/mL were placed in the upper chambers in 0.3ml 5% serum media, and the lower chambers were added with 0.6 mL LPS 50 ng.mL^{-1}, 1.0 μM DHA+LPS 50 ng.mL^{-1}, 4.0μM DHA+ LPS 5050 ng.mL^{-1}, or 10% serum DMEM as negative control. Cells were allowed to transmigrate into the lower chamber following incubation for 12 h at 37°C; nonmigrating cells on the upper chamber surface were removed. The membranes were fixed with 4% paraformaldehyde in PBS for 30 min and stained with crystal violet in PBS for 15 min. The representative images (magnification, ×200) were randomly taken by an inverted microscope. Each experimental group was repeated three times.

ELISA for CCL5 detection

Serum and cerebrospinal fluid were taken at the day 26 and culture supernatants from BV2 cells were evaluated using ELISA kit (all from proteintech, USA) according to the manufacturer’s instructions.

Statistical analysis

Data was analyzed using GraphPad Prism 7 software (GraphPad, La Jolla, CA, USA), and was presented as the mean ± SEM. Significant differences in comparing multiple groups, data were analyzed by one-way ANOVA test. All other statistical comparisons were done using nonparametric statistical tests. Differences with p values of less than 0.05 were considered significant.

Results

1. DHA is a promising candidate showing some therapeutic advantages in EAE

Firstly, we identified the therapeutic effect of DHA on the development and severity of mice with EAE. The onset of clinical signs began on the 4th day postimmunization. As time went on, in EAE group, all mice had developed clinical symptoms and the mean clinical score was 3.92 ± 0.25 on the 18th day at the peak of the disease, also accompanied by paralysis of all four limb. In contrast, the mean clinical score in the DHA 10 mg.kg^{-1} treated group (1.98 ± 0.21) was significantly reduced to nearly two-fold. Strikingly, the disease score was even less than one-fold than treatment with MET (2.84 ± 0.19), the most widely used drug for MS in the clinical treatment (Fig. 1A). Besides, DHA treatment obviously prevented the body

weight loss in EAE mice (Fig. 1B). These results predicted that DHA had therapeutic potential in preventing EAE.

Histologically, to make further effort to DHA efficacy verification, spinal cord and brain tissue sections were prepared and then H&E staining was performed. Results in Fig. 1C and D showed that DHA significantly inhibited the pathological infiltration of inflammatory cells. Then, to histologically detect the protective effect on myelin, we used Luxol Fast Blue (LFB) staining, a specific myelin detection method. In EAE group, result in Fig. 1E showed the intensity of LFB staining in corpus callosum was weakened, most myelin lipids were pale blue, and blue filaments were hardly visible at the edge of spinal cord which can be seen as marker of demyelination. By contrast, DHA treatment remarkably prevented the demyelination.

Morphologically, we directly observed the ultramicroscopic structure of pathological changes by using transmission electron microscopic. Result in Fig. 1F showed an "orbital like" compact lamellar structure with no shrinkage, tightly arranged myelin sheath in negative control group. The impaired axons and inner vacuoles were also rarely observed. On the contrary, in EAE group, there were obvious pathological changes in the myelin sheath, the shape of myelin sheath was irregular, the lamella of myelin sheath was obviously loose, disintegrated, fused, or even lost. Consistent with previous results, the damages in myelin, as quantified by demyelinating or intact areas of nerve fibers, could be significantly prevented after DHA 10 $mg.kg^{-1}$ treatment, which even showed more protective effects than MET group.

Of note, by using gait analysis, we for the first time verified the efficacy of DHA. Results were shown in Fig. 1G. DHA treatment can obviously reverse the disorder of walk speed, Lh-Rh Pressure, Lh-Rh support time, Lh-Rh Print area, and ameliorate Body Rotation Average. Furthermore, it showed more therapeutic effects than MET in the perspective of walk speed and Lh-Rh Pressure. In conclusion, results from different aspects convinced us the therapeutic significance of DHA on EAE mice, which supported its future application in MS.

2. AXL in microglia was the potential responsive molecule of DHA in EAE

To detect the drug-responsive cell subset in 10x Genomics, we firstly used tSNE (t-Distributed Stochastic Neighbor Embedding) projection. Then, we used Louvain optimization algorithm to cluster and classify the cell groups. The responsive cell-types to DHA can finally be categorized into 14 sub-populations. Among them, Macrophage and microglia were for the first time identified as the most responsive cells and illustrated by graph-based clustering (Fig. 2A).

Furthermore, we also geonomy-widely provided the description for the DHA responsive molecular network and screened the specific marker genes expression in microglia. Result indicated that AXL was specifically induced by DHA in microglia from EAE mice. Pathologically, gene deficiency of AXL in EAE would cause much more excessive autoimmune inflammatory reaction, consequently inducing myelin

sheath damage [30]. This study gave us great inspiration and reliable evidence that AXL may be a potential target for DHA treatment (Fig. 2B).

3. The inflammatory–resolving effect of DHA is functionally correlated with AXL

To immunologically elucidate DHA mediated resolution of autoimmune inflammation, the AXL-concentrated efficacy analysis was functionally conducted mainly through three aspects. These included the regulation of phagocytic and chemotactic potential in microglia as well as the regulation in co-regulatory signaling during antigen-presentation.

Firstly, to identify the prediction from 10x Genomics, we quantified the transcription level of AXL in mononuclear cells (MNCS) collected from CNS tissues in EAE mice, whose total number reflects the degree of infiltrated inflammatory cells [21]. As shown in Fig. 3A, by qRT-PCR assay, DHA treatment can up-regulate the expression of AXL compared with the vehicle control group. In contrast, GAS6, the ligand for AXL, showed no differences among each group (Fig. 3B). Consistent with the transcriptional result, the protein expression of AXL was further detected. Results showed that (Fig. 3C and D), specifically under inflammatory condition, DHA can up-regulate AXL compared with modeling group.

As indicated by previous report, relying on AXL, microglia can sense and engulf apoptotic cells, clear the myelin debris in CNS. Facilitating by such mechanism, the over-activated inflammation can be rapidly resolved and effectively confined within a small area. We therefore, functionally evaluated the impact of DHA on phagocytosis of microglia in vitro. In this study, the 5-Fu induced apoptotic PC12 cells (the apoptosis rate: more than 81%, Fig. 3E) were co-cultured with BV2 cells and the phagocytotic intensities were quantified by flow cytometry and further visualized by microscopic observation. As shown in Fig. 3F and G, compared with LPS group, the count and percentage of PC12 cells phagocytized by BV2 cells in DHA (1.0/4.0 μM) groups were both significantly increased. This result proved that the phagocytic ability of microglia under inflammation condition can be significantly enhanced by DHA, forming the important basis for inflammation resolution.

In the next study, from the perspective of “antigen uptake and presentation”, we aim to reveal the influence of DHA on APCs. Inspired by the essential roles of co-regulatory factors during EAE progression, detection of PDL1 and CD80 were chosen as the markers for the immunological properties during antigen presentation. As shown in Fig. 4A and B, in both Raw264.7 cells and peritoneal macrophages, DHA obviously increased the transcription of PDL1 compared with LPS treated group. However, there are no changes in the transcription of CD80 between DHA and LPS treated groups. Consistently, Flow cytometry analysis showed that the enhanced surface expression of PDL1 can be clearly detected in DHA treated macrophages as well as BV2 microglia cell lines (Fig. 4C, D and E). These results provided molecular indications that, by upregulating PDL1 in microglia, DHA showed potential for enhancing the co-inhibitory

signaling during antigen presentation and neutralizing the excessive inflammatory signals in the progression of autoimmune diseases.

To further detect whether DHA directly influences the differentiation of T cells, we established a co-culture model of BV2-Jurkat T cells. Results in Fig. 4F showed that DHA (1.0/4.0 μM) significantly elevated the percentage of Treg cells (CD4 + Foxp3+), compared with LPS group. These results showed that DHA suppressed autoimmune inflammation partially through enhancing of PDL1 expression and promoting the differentiation of Treg cells.

According to the indication from the 10x Genomics, CCL5 is one of the most responsive molecules in DHA treatment (Fig. 5A and B). Inspired by the crucial role of CCL5 in the trafficking of encephalitogenic T cells, we firstly analyzed the level of CCL5 by using the qRT-PCR and ELISA assays (Fig. 5C). In line with the geonomy-wide screening, DHA treatment can obviously inhibit the gene expression in MNCS separated from EAE mice. Besides, the high level of CCL5 in the cerebrospinal fluid (CSF) of EAE mice can also be significantly reversed by DHA treatment (Fig. 5D). which shows the same pattern in the serum (Fig. 5E).

To functionally determine the influence of DHA on the chemoattraction of microglia, we used LPS to induce the production of CCL5 for 12 hours. Next, the supernatant was collected for the detection of CCL5 concentration by using ELISA assay. The results in Fig. 5F showed that DHA treatment can obviously reduce LPS-stimulated CCL5 secretion. Trans-well assay showed that DHA (1.0/4.0 μM) dramatically reduced the chemotactic ability of BV2 cells in LPS treated model (Fig. 5G).

4. The inflammatory-resolving effects of DHA necessitated the AXL signaling in microglia

Molecularly, in order to clarify whether the inhibition of autoimmune inflammation of DHA is required for the presence of AXL. We used SGI7079, the phosphorylation blocker of AXL at Tyr702. Figure 6A demonstrated that challenging with SGI7079 successfully blocked phosphorylation of AXL and the related regulation on STAT1:SOCS3 pathway. In addition, Fig. 6 also implied SGI7079 is sufficient to neutralize the inflammation resolving effects of DHA in microglia. The T cell differentiation (Fig. 6B, C), phagocytic potential (Fig. 6D, E) and chemotactic sensitivity (Fig. 6F, G) consistently showed no statistical differences among DHA, LPS and NC treated group ($P > 0.05$), indicating that AXL would be a potential target of DHA in treating EAE.

5. DHA specifically rebalanced overactivated inflammation by regulating AXL related STAT1:SOCS3 pathway

Large amounts of researchers have found that, specifically under the pro-inflammatory conditions, AXL interacted with type I interferon receptor (IFNAR) and potentiated the downstream inflammatory-resolving

events as represented by the activation of STAT1:SOCS3 pathway. Of great interest, as the molecular switch for inflammation from promotion to resolution, the transcription of AXL itself is inversely facilitated by STAT1, a central inflammatory sensor regulated by various types of pro-inflammatory signals including IFN-β ligation to IFNAR. This forms the endogenous basis for the negative feedback loop of immune responses and consequently maintains the homeostasis in inflammatory microenvironment (graphically shown in below, Fig. 7.).

In light of this, to molecularly clarify the mechanistic revelation of DHA to IFNAR- STAT1 pathway, inflammatory stimulator to IFNAR (LPS or more specifically, IFN-β) were used and the influences of DHA on this pathway were then evaluated in BV2 cells. As shown in Fig. 8, in the presence of DHA, the expression of AXL can be dramatically induced by both LPS (Fig. 8A and D) and IFN-β (Fig. 8B and E), leading to a molecular pattern with higher inflammation-resolution potential, as suggested by SOCS3 upregulation. Moreover, in sharp contrast to the results obtained from the STAT1-avaliable state, the expression of AXL and SOCS3 were kept at the similar levels comparing to modeling group when phosphorylation of STAT1 was blocked by Fludarabine (FLU) (Fig. 8C and F). This result revealed that the enhanced AXL expression and the negative regulation of DHA in inflamed microglia were both required for the normal-responsiveness of STAT1 pathway.

Next, recent findings further proved that the inflammatory resolution effects of AXL shows high specificity to proinflammation conditions, which suggested that the biological activities of AXL were integrated into the IFN-β-IFNAR activation. To test such specificity, in the non-inflamed state, the STAT1:SOCS3 pathway was analyzed in the presence of DHA. In addition, the inflammatory resolving functions mediated by AXL were phenotypically measured in DHA treated BV2 cells. As shown in Fig. 9A, without inflammatory stimulation, DHA failed to regulate STAT1-SOCS3 pathway. Functionally, the differentiation induction of Treg cells (Fig. 9B, C), phagocytic (Fig. 9D) and chemotactic influences of BV2 cells (Fig. 9E), as above-proved manipulated by DHA, were totally neutralized. These results indicated that DHA functions as a resolution promoter by regulating AXL related STAT1:SOCS3 pathway specifically in the condition of over-activated inflammation.

Discussion

Previous studies indicated that there may exist close correlation between DHA and T cells differentiation in treating autoimmune inflammation, leaving large research gap for the systematic understanding about its immunological activities, especially the molecular explanation for the regulation of Th17/Treg balance[24]. In our study, inspired by cell-type based recognition and characterization, we for the first time identified macrophage/microglia as the most responsive cells of DHA in autoimmune-inflammation lesion of EAE model. This finding largely expanded the traditional concept holding that the anti-inflammatory effects of DHA was limited in T cells regulation.

Recent researches have proved that microglia actively participate in almost all MS processes. It serves as the major immune-active element and pioneer cells in the inflamed CNS. Therefore, modulating the function of microglia can be an attractive therapeutic strategy in coping with CNS inflammation and inflammation-induced demyelination[30]. More importantly, supported by geonomy-wide sequencing and bioinformatics analysis, we for the first time revealed that AXL was proved to be the potential responsive gene functionally executing the pro-resolution effects of DHA, as demonstrated by the elevated phagocytosis, chemotactic inhibition and co-inhibitory signaling enhancement in microglia from EAE model. This result provided indicative evidences for the deeper understanding of DHA in activating the endogenous self-limitation mechanism during the progression of autoimmune inflammation. Furthermore, it also revealed a theoretical explanation for the DHA-mediated Treg differentiation as reported by previous researchers.

Relying on the regulatory effect in STAT1:SOCS3 signaling and the direct interaction with IFNAR, AXL was identified as a switch in mediating inflammatory transition from promotion to resolution and a crucial maintainer for immune homeostasis. Pathologically, the functional defect of AXL and its abnormal regulation in STAT1-transduced signaling cascades form part of the molecular basis attributing to autoimmune disease progression, especially in MS[18]. In our study, by combining genome-wide screening with molecular biological analysis, we obtained convincing evidence in targeting AXL by DHA. In clear contrast to MET, the most commonly-used drugs for MS in clinic, our research demonstrated that DHA may not be a unidirectional and immoderate immunosuppressant. Instead, DHA is a potential inflammation-conditioned rebalancer, featuring “No inflammation, No inhibition” properties. Such hypothesis can be experimentally supported in our study. When the inflammation was pathologically over-activated, DHA may enhance the IFNAR- AXL interaction and promoted inflammation resolution through transducing signals to STAT1:SOCS3. By contrast, as the inflammation tends to be mitigated, the induction of AXL and activation of SOCS3 were weakened due to the dissociation between INFAR-AXL and the deactivation of IFNAR: STAT1 pathway, which do not further induce sustained over-suppression of the immune response (as proved by Fig. 9).

Hopefully, this mechanistic feature initially indicated the advantages of DHA in treating EAE, suggesting that DHA may be a promising candidate in glucocorticoids-alternative therapeutic strategy. By DHA application, it may also be helpful to avoid the side effects of glucocorticoid, including prednisone, methylprednisolone, and betamethasone, causing excessive immune suppression. To further reveal the therapeutic significance of DHA, the specific mechanisms and validation of pharmacodynamic dependence of DHA and AXL would become the key research project in our future study.

Conclusions

We for the first time highlighted that, by enhancing AXL signaling, DHA efficiently blocked the inflammatory initiation and expansion in EAE as proved by the reduced chemoattraction, the induction of Treg differentiation and the enhanced efferocytosis of microglia, contributing to autoimmune homeostasis. Our study pharmacologically indicated that, specifically when inflammation was

overactivated, DHA may be a promising candidate for the treatment of EAE. We also proved DHA may show more favorable efficacy comparing with glucocorticoids in MS treatment.

Abbreviations

APCs: antigen presentation cells

AXL: Anexelekto

CNS: central nervous system

CCL5(RANTES): regulated upon activation normal T cell expressed and secreted factor

DHA: Dihydroartemisinin

EAE: Experimental Autoimmune Encephalomyelitis

GAS6: growth arrest specific gene 6

MS: Multiple Sclerosis

PDL1: Programmed cell death ligand 1

STAT1: signal transducer and activator of transcription 1

SOCS3: suppress of cytokine signaling 3

TEM: Transmission Electron Microscopy

Declarations

Ethics Statement

All animal experiments were approved by the local Laboratory Animal Ethics

Committee of the Institute of basic theory of traditional Chinese medicine, of the China Academy of Chinese Medical Sciences (license number SCXK 2016-0021) and performed in accordance with the guidelines for the care and use of laboratory animals.

Competing interests

The funding agency had no role in study design, data collection and analysis, decision to publish or preparation of the manuscript. The authors have no financial or non-financial competing interests to declare.

Author contribution

Qingsen Ran and Qi Li participated in the manuscript writing and experimental design and performed the experiments. Lidong Sun and Li Liu participated in performing parts of the experiments. Qing Yang, Yujie Li, Ying Chen, Xiaogang Weng, Yajie Wang, Weiyan Cai participated in the manuscript writing, manuscript editing and data analysis. Xiaoxin, Zhu participated in the manuscript writing, experimental design and data analysis. All authors have read and approved the manuscript.

Funding

This work was supported by grants from National High Technology Research and Development Program of China (2017ZX09101002-002-002); Institute of traditional Chinese medicine internal project- the research on reevaluating traditional Chinese medicine based on antibiotic substitution (NO. Z2017019-03); “the Belt and Road” cooperation project of China academy of traditional Chinese medicine (NO. GH201914); The General Programs of the National Natural Science Foundation of China (8157141621); Special training program for outstanding young scientific and technological talents of China academy of Chinese Medical Science (ZZ13-YQ-044); Independent topic selection project China academy of Chinese Medical Science (ZXKT17010); China academy of traditional Chinese medicine internal project—Construction of China-European research center for traditional Chinese medicine and natural products (NO. GH2017-01).

Consent for Publication

Not applicable

Availability of supporting data

The datasets used or analyzed during the current study are available from the corresponding author on reasonable request.

Acknowledgements

Grateful acknowledgement is made to my supervisor professor Xiaoxin Zhu who gave me considerable help by means of suggestion, comments and criticism. His encouragement and unwavering support have sustained me through frustration and depression. Without his pushing me ahead, the completion of this thesis would be impossible. In addition, I deeply appreciate the contribution to this thesis made in various ways by my friends and classmates.

References

1. Reich DS, Lucchinetti CF, Calabresi PA. Multiple Sclerosis. *N Engl J Med* 2018; 378: 169-80.
2. Glatigny S, Bettelli E. Experimental Autoimmune Encephalomyelitis (EAE) as Animal Models of Multiple Sclerosis (MS). *Cold Spring Harb Perspect Med* 2018; 8.
3. Jalosinski M, Karolczak K, Mazurek A, Glabinski A. The effects of methylprednisolone and mitoxantrone on CCL5-induced migration of lymphocytes in multiple sclerosis. *Acta Neurol Scand* 2008; 118: 120-5.
4. Vainchtein ID, Vinet J, Brouwer N, Brendecke S, Biagini G, Biber K*, et al.* In acute experimental autoimmune encephalomyelitis, infiltrating macrophages are immune activated, whereas microglia remain immune suppressed. *Glia* 2014; 62: 1724-35.
5. Monsonego A, Imitola J, Zota V, Oida T, Weiner HL. Microglia-mediated nitric oxide cytotoxicity of T cells following amyloid beta-peptide presentation to Th1 cells. *J Immunol* 2003; 171: 2216-24.
6. Voet S, Prinz M, van Loo G. Microglia in Central Nervous System Inflammation and Multiple Sclerosis Pathology. *Trends Mol Med* 2019; 25: 112-23.
7. O'Loughlin E, Madore C, Lassmann H, Butovsky O. Microglial Phenotypes and Functions in Multiple Sclerosis. *Cold Spring Harb Perspect Med* 2018; 8.
8. Saijo K, Glass CK. Microglial cell origin and phenotypes in health and disease. *Nat Rev Immunol* 2011; 11: 775-87.
9. Li X, Zhao L, Han JJ, Zhang F, Liu S, Zhu L*, et al.* Carnosol Modulates Th17 Cell Differentiation and Microglial Switch in Experimental Autoimmune Encephalomyelitis. *Front Immunol* 2018; 9: 1807.
10. Togno-Peirce C, Nava-Castro K, Terrazas LI, Morales-Montor J. Sex-associated expression of co-stimulatory molecules CD80, CD86, and accessory molecules, PDL-1, PDL-2 and MHC-II, in F480+ macrophages during murine cysticercosis. *Biomed Res Int* 2013; 2013: 570158.
11. Szczucinski A, Losy J. Chemokines and chemokine receptors in multiple sclerosis. Potential targets for new therapies. *Acta Neurol Scand* 2007; 115: 137-46.
12. Martin-Blondel G, Brassat D, Bauer J, Lassmann H, Liblau RS. CCR5 blockade for neuroinflammatory diseases--beyond control of HIV. *Nat Rev Neurol* 2016; 12: 95-105.
13. Cheng X, Zhao Z, Ventura E, Gran B, Shindler KS, Rostami A. The PD-1/PD-L pathway is up-regulated during IL-12-induced suppression of EAE mediated by IFN-gamma. *J Neuroimmunol* 2007; 185: 75-86.
14. Carter LL, Leach MW, Azoitei ML, Cui J, Pelker JW, Jussif J*, et al.* PD-1/PD-L1, but not PD-1/PD-L2, interactions regulate the severity of experimental autoimmune encephalomyelitis. *J Neuroimmunol* 2007; 182: 124-34.
15. Zhang Q, Vignali DA. Co-stimulatory and Co-inhibitory Pathways in Autoimmunity. *Immunity* 2016; 44: 1034-51.
16. Shafit-Zagardo B, Gruber RC, DuBois JC. The role of TAM family receptors and ligands in the nervous system: From development to pathobiology. *Pharmacol Ther* 2018; 188: 97-117.
17. Korshunov VA. Axl-dependent signalling: a clinical update. *Clin Sci (Lond)* 2012; 122: 361-8.

18. Rothlin CV, Ghosh S, Zuniga EI, Oldstone MB, Lemke G. TAM receptors are pleiotropic inhibitors of the innate immune response. *Cell* 2007; 131: 1124-36.
19. Lemke G, Rothlin CV. Immunobiology of the TAM receptors. *Nat Rev Immunol* 2008; 8: 327-36.
20. Fourgeaud L, Traves PG, Tufail Y, Leal-Bailey H, Lew ED, Burrola PG*, et al.* TAM receptors regulate multiple features of microglial physiology. *Nature* 2016; 532: 240-44.
21. Kasikara C, Kumar S, Kimani S, Tsou WI, Geng K, Davra V*, et al.* Phosphatidylserine Sensing by TAM Receptors Regulates AKT-Dependent Chemoresistance and PD-L1 Expression. *Mol Cancer Res* 2017; 15: 753-64.
22. Lemke G, Burstyn-Cohen T. TAM receptors and the clearance of apoptotic cells. *Ann N Y Acad Sci* 2010; 1209: 23-9.
23. Wu Y, Tang W, Zuo J. Development of artemisinin drugs in the treatment of autoimmune diseases. *Science Bulletin* 2016; 61: 37-41.
24. Zhao YG, Wang Y, Guo Z, Gu AD, Dan HC, Baldwin AS*, et al.* Dihydroartemisinin ameliorates inflammatory disease by its reciprocal effects on Th and regulatory T cell function via modulating the mammalian target of rapamycin pathway. *J Immunol* 2012; 189: 4417-25.
25. Shi Z, Chen Y, Lu C, Dong LM, Lv JW, Tuo QH*, et al.* Resolving neuroinflammation, the therapeutic potential of the anti-malaria drug family of artemisinin. *Pharmacol Res* 2018; 136: 172-80.
26. Liu H, Tian Q, Ai X, Qin Y, Yang CJO. Dihydroartemisinin attenuates autoimmune thyroiditis by inhibiting the CXCR3/PI3K/AKT/NF-κB signaling pathway 2017; 8: 115028-40.
27. Li SD, Shi Z, Zhang H, Liu XM, Chen SG, Jin J*, et al.* Assessing gait impairment after permanent middle cerebral artery occlusion in rats using an automated computer-aided control system 2013; 250: 174-91.
28. McArthur S, Cristante E, Paterno M, Christian H, Roncaroli F, Gillies GE*, et al.* Annexin A1: a central player in the anti-inflammatory and neuroprotective role of microglia. *J Immunol* 2010; 185: 6317-28.
29. Hodzic EJBJBM. Single-cell analysis: Advances and future perspectives 2016.
30. Weinger JG, Brosnan CF, Loudig O, Goldberg MF, Macian F, Arnett HA*, et al.* Loss of the receptor tyrosine kinase Axl leads to enhanced inflammation in the CNS and delayed removal of myelin debris during experimental autoimmune encephalomyelitis. *J Neuroinflammation* 2011; 8: 49.

Supplementary Information

Supplementary data 1 was not provided with this version of the manuscript.

Figures

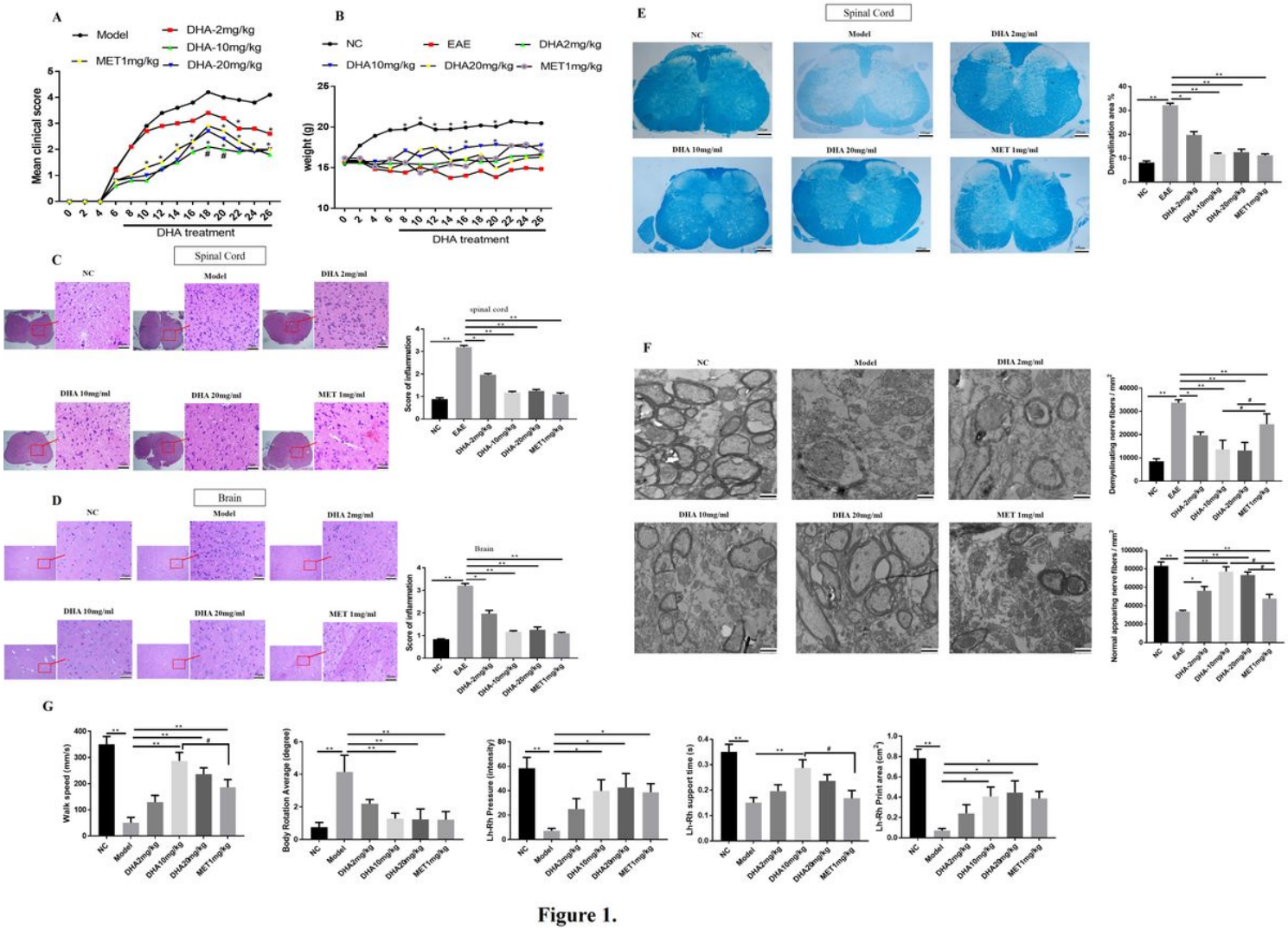

Figure 1.

Figure 1

DHA is a promising candidate showing some therapeutic advantages in EAE A, B) Mean clinical scores and weight of EAE mice that were i.g. daily with DHA (2, 10, 20 mg.kg-1), MET(1mg.kg-1) or vehicle control from day 7 (n=10, preventive treatment) post immunization onwards. C, D, E) Transverse sections of brains spinal cords from control EAE mice and DHA-treated mice were stained with H&E (40× and 100×) or LFB (40×). Histopathology score of CNS inflammation and demyelination was quantified using H&E and LFB staining on day 26 post immunization. F) TEM images (15000×) showed demyelinated axons in the spinal cords of control EAE, MET-treated and DHA-treated mice on day 26. G) Gait analysis (walk speed; Body Rotation Average; Lh-Rh Pressure; Lh-Rh support time; Lh-Rh Print area) of control EAE, MET-treated and DHA-treated mice from day 20 to day 26. Data are representative of three independent experiments. *P=<0.05; **P=<0.01; compared with MET treated group, #P=<0.05; ns=no statistical significance. MET= methylprednisolone; Lh=Left hindpaw; Rh= Right hindpaw.

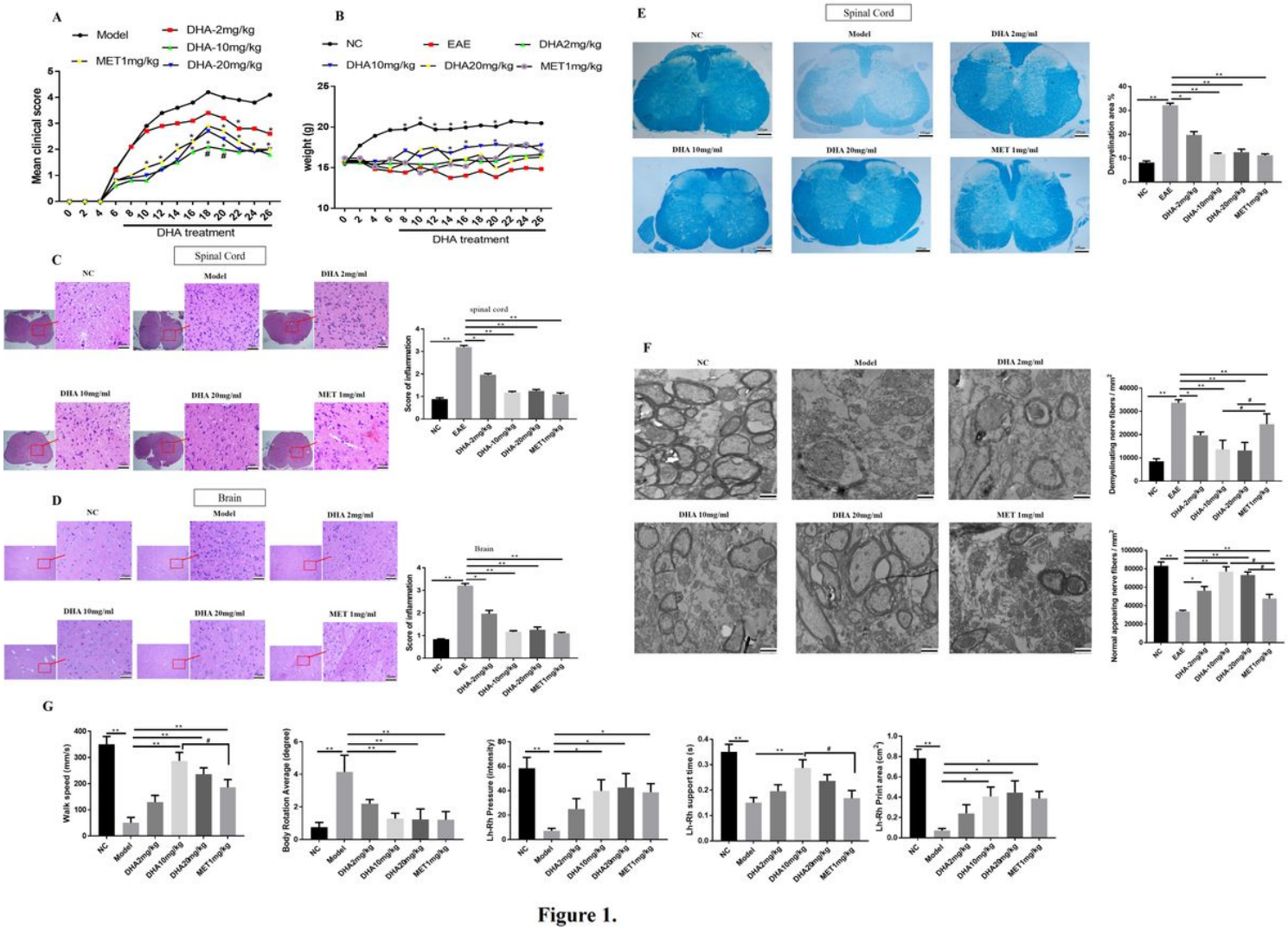

Figure 1.

Figure 1

DHA is a promising candidate showing some therapeutic advantages in EAE A, B) Mean clinical scores and weight of EAE mice that were i.g. daily with DHA (2, 10, 20 mg.kg-1), MET(1mg.kg-1) or vehicle control from day 7 (n=10, preventive treatment) post immunization onwards. C, D, E) Transverse sections of brains spinal cords from control EAE mice and DHA-treated mice were stained with H&E (40× and 100×) or LFB (40×). Histopathology score of CNS inflammation and demyelination was quantified using H&E and LFB staining on day 26 post immunization. F) TEM images (15000×) showed demyelinated axons in the spinal cords of control EAE, MET-treated and DHA-treated mice on day 26. G) Gait analysis (walk speed; Body Rotation Average; Lh-Rh Pressure; Lh-Rh support time; Lh-Rh Print area) of control EAE, MET-treated and DHA-treated mice from day 20 to day 26. Data are representative of three independent experiments. *P=<0.05; **P=<0.01; compared with MET treated group, #P=<0.05; ns=no statistical significance. MET= methylprednisolone; Lh=Left hindpaw; Rh= Right hindpaw.

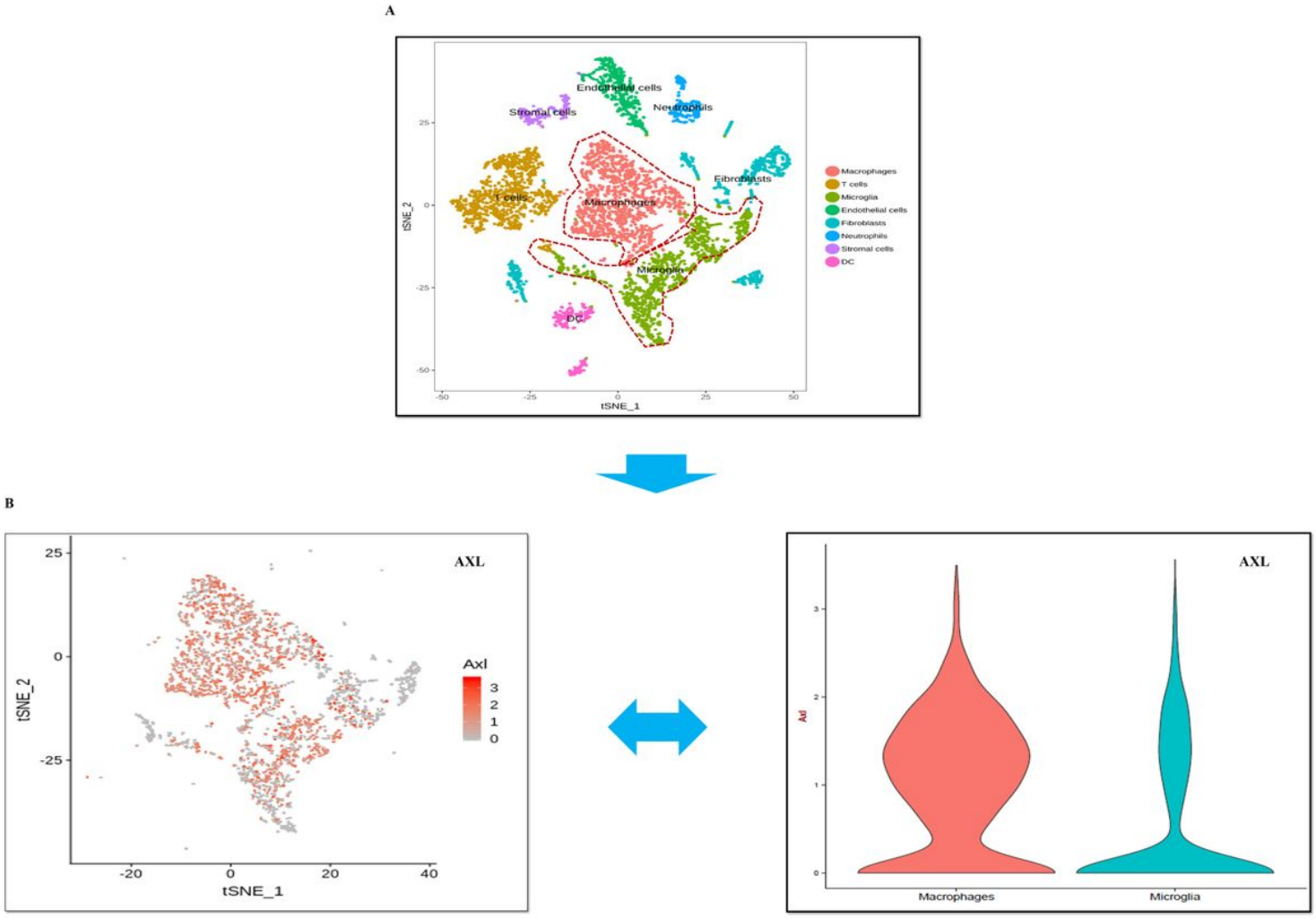

Figure 2.

Figure 2

AXL in microglia was the potential responsive molecule of DHA in EAE A) The t-SNE projection of scRNA-seq data showed clusters of cells which would response to the disease in EAE mice. B) CNV analysis showed that AXL was almost expressed in macrophages and microglia (red, cells with detected CNVs; gray, no detected CNVs). Data are representative of three independent experiments. *P=<0.05; **P=<0.01; ns=no statistical significance.

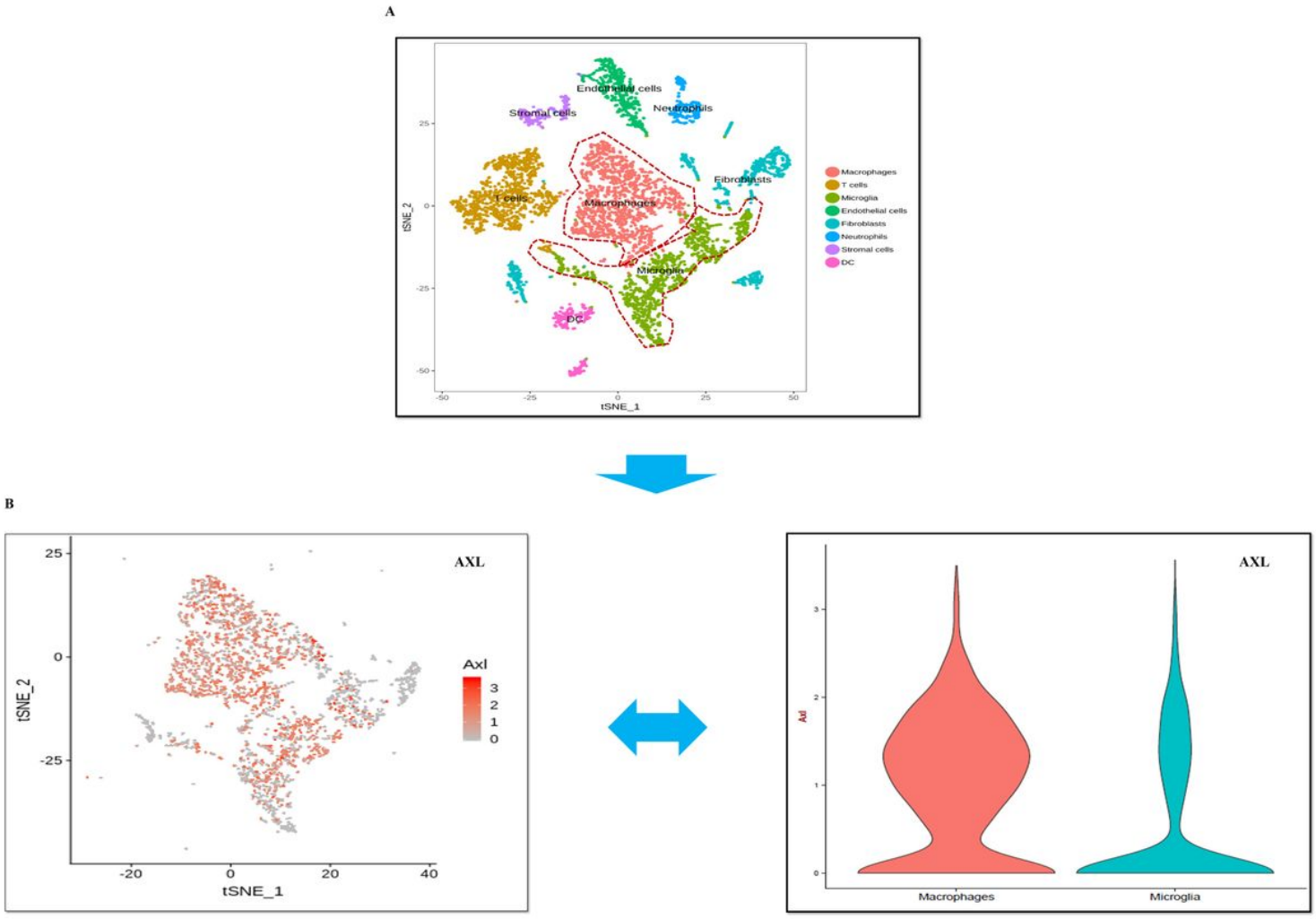

Figure 2.

Figure 2

AXL in microglia was the potential responsive molecule of DHA in EAE A) The t-SNE projection of scRNA-seq data showed clusters of cells which would response to the disease in EAE mice. B) CNV analysis showed that AXL was almost expressed in macrophages and microglia (red, cells with detected CNVs; gray, no detected CNVs). Data are representative of three independent experiments. *P=<0.05; **P=<0.01; ns=no statistical significance.

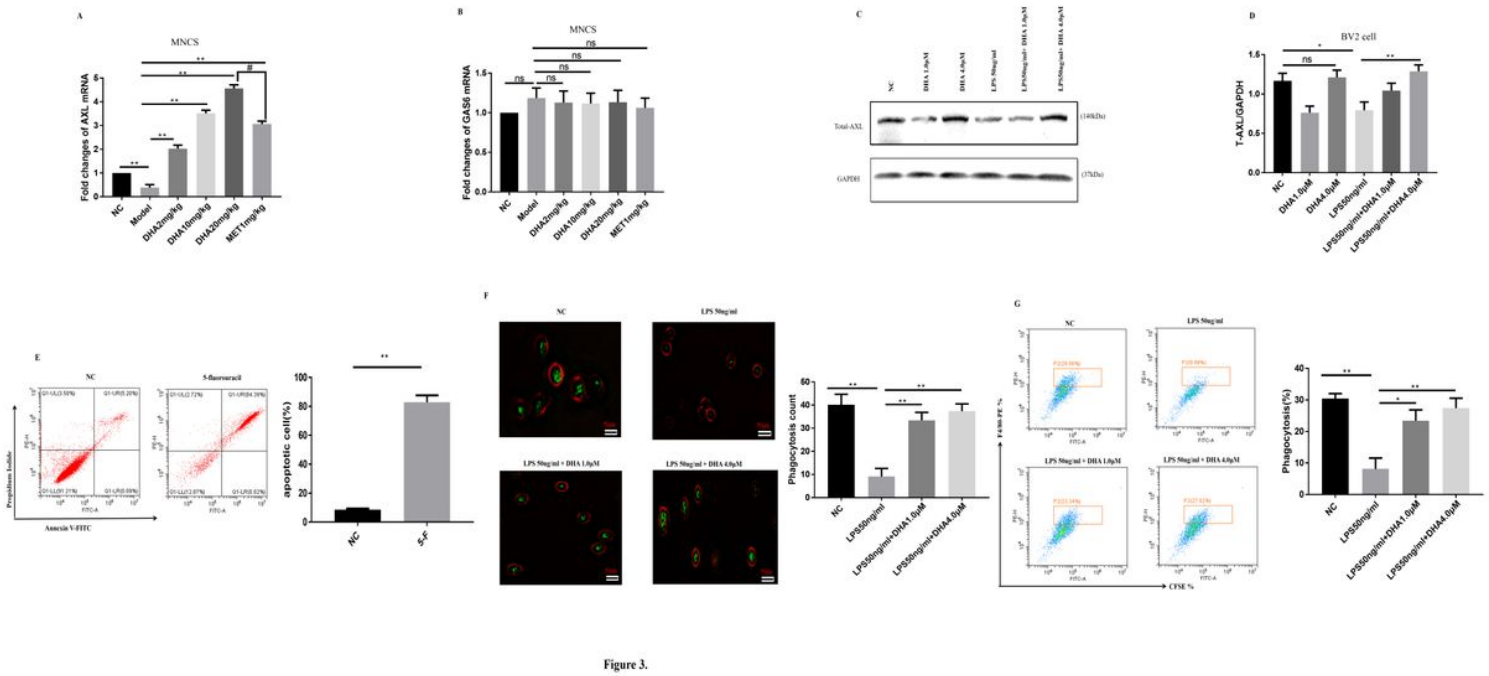

Figure 3.

Figure 3

The inflammatory –resolving effects of DHA is functionally correlated with AXL MNCS from EAE, MET(1mg.kg-1) and DHA (2, 10, 20 mg.kg-1) mice were harvested by 30/70% percoll gradient separation. A, B) qRT-PCR assay for AXL and GAS6 were analyzed by LightCycler 480 Ⅱ Roche. C, D) Western blot analysis for AXL expression in BV2 cells under the treatment of LPS (50ng.ml-1) and DHA (1.0/4.0μM). E) We used 5-F to induced the apoptosis of PC12 cells, AV-PI analysis showed the 5-F could induce the apoptosis of PC12 cells. PC12 cells were then transferred into BV2 cells for 2h. F, G) Fluorescence microscope images (400×) showed count of phagocyting apoptosis cell by BV2 cells (green represent PC12 cells; red represent BV2 cells) and Flow cytometry assay showed the percent of phagocytosis cell (CYSE+/F480+). Data are representative of three independent experiments. *P=<0.05; **P=<0.01; compared with MET treated group; #P=<0.05; ns=no statistical significance. 5-F=5-fluorouracil.

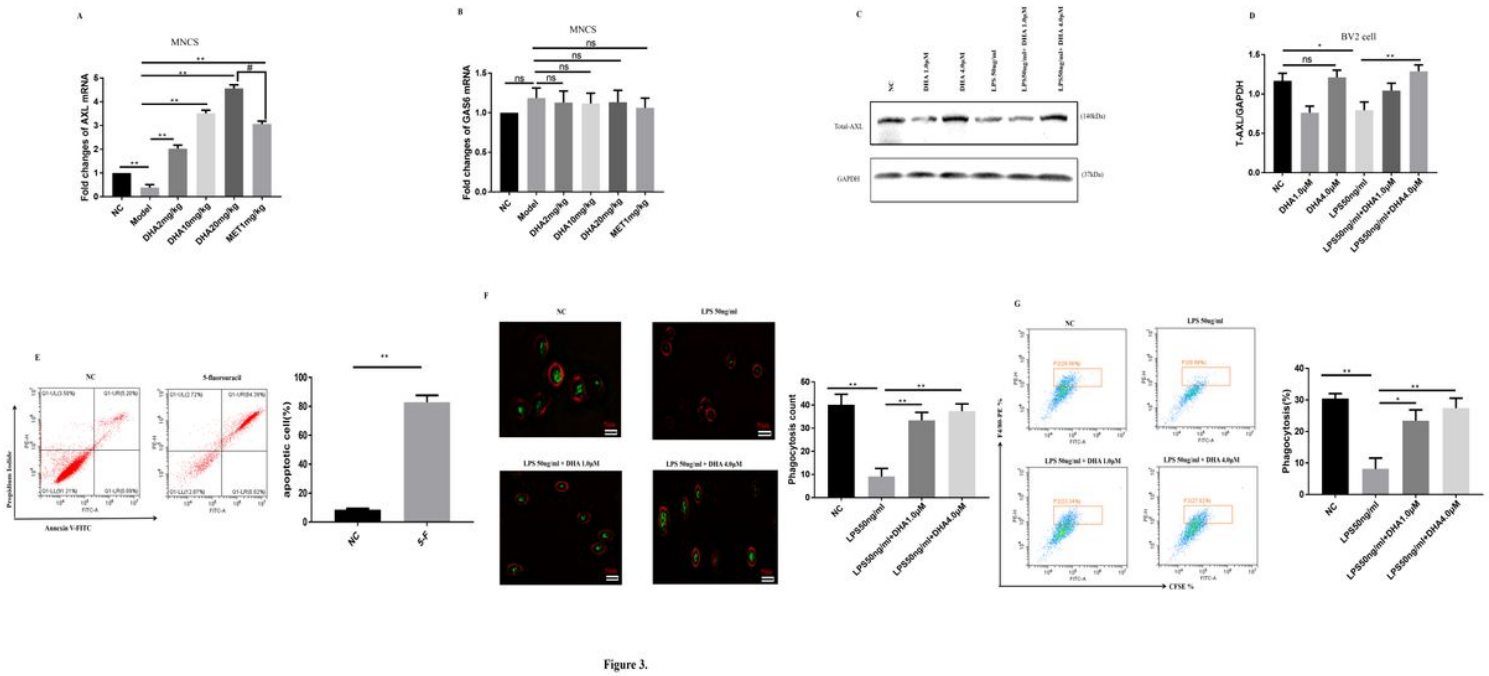

Figure 3.

Figure 3

The inflammatory –resolving effects of DHA is functionally correlated with AXL MNCS from EAE, MET(1mg.kg-1) and DHA (2, 10, 20 mg.kg-1) mice were harvested by 30/70% percoll gradient separation. A, B) qRT-PCR assay for AXL and GAS6 were analyzed by LightCycler 480 Ⅱ Roche. C, D) Western blot analysis for AXL expression in BV2 cells under the treatment of LPS (50ng.ml-1) and DHA (1.0/4.0μM). E) We used 5-F to induced the apoptosis of PC12 cells, AV-PI analysis showed the 5-F could induce the apoptosis of PC12 cells. PC12 cells were then transferred into BV2 cells for 2h. F, G) Fluorescence microscope images (400×) showed count of phagocyting apoptosis cell by BV2 cells (green represent PC12 cells; red represent BV2 cells) and Flow cytometry assay showed the percent of phagocytosis cell (CYSE+/F480+). Data are representative of three independent experiments. *P=<0.05; **P=<0.01; compared with MET treated group; #P=<0.05; ns=no statistical significance. 5-F=5-fluorouracil.

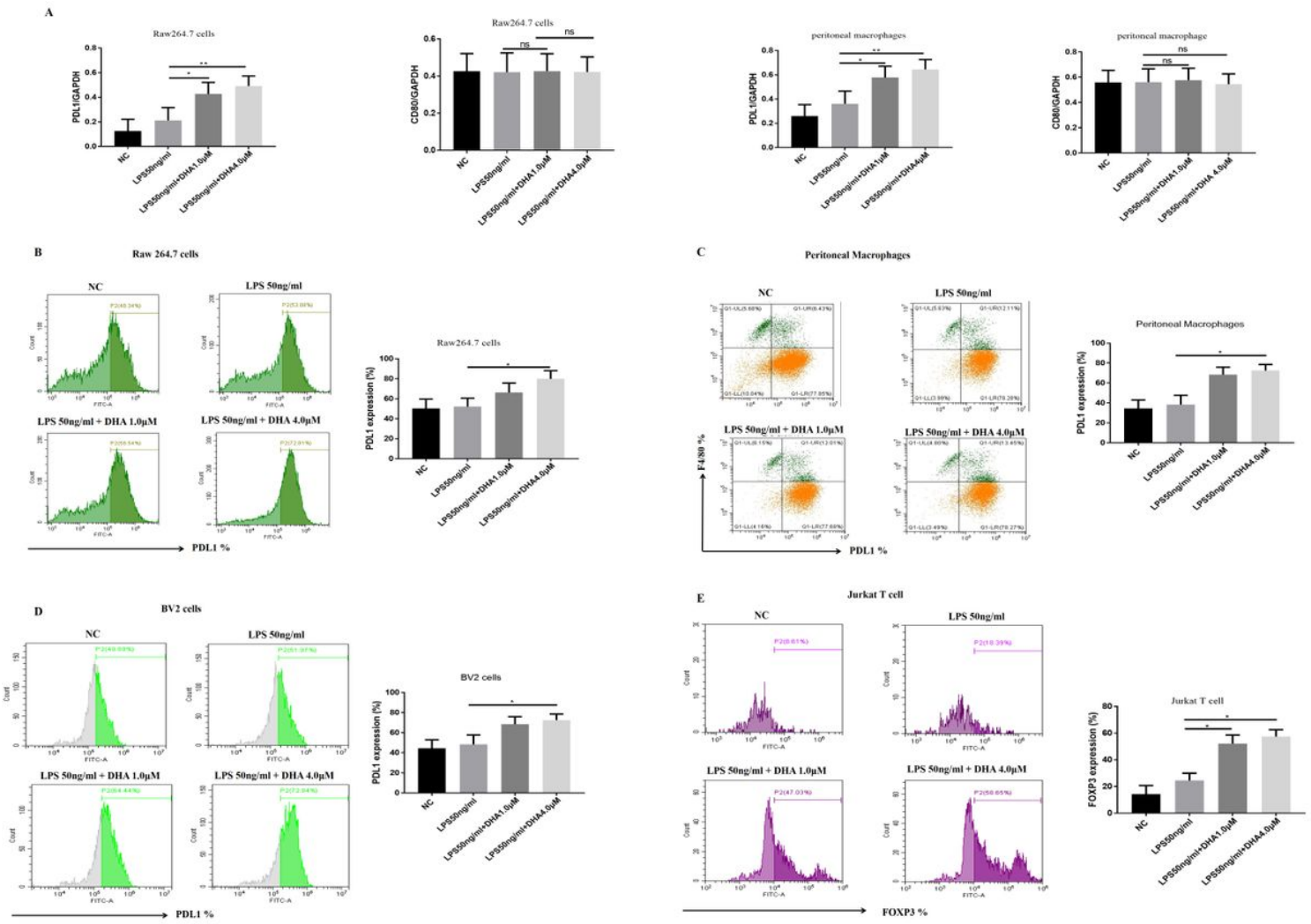

Figure 4.

Figure 4

The inflammatory –resolving effects of DHA is functionally correlated with AXL Peritoneal macrophages from C57BL/6 mice were challenged by 3% sodium thioglycolate three days in advance. A) RT-PCR analysis for PDL1 and CD80 transcription in Raw 264.7 cells and peritoneal macrophages which were treated by LPS (50ng.ml-1) and DHA (1.0/4.0μM). B, C, D) Flow cytometry assay for PDL1 expression in Raw 264.7 cells, peritoneal macrophages (PDL1+/F480+) and BV2 cells by LPS (50ng.ml-1) and DHA (1.0/4.0μM) treatment. BV2 cells were treated by DHA (1.0/4.0μM) or LPS (50ng.ml-1) for 12h, and then Jurkat T cells were co-cultured with BV2 cells for another 12h. E) FOXP3 expression on Jurkat T cells analyzed by flow cytometry. Data are representative of three independent experiments. *P=<0.05; **P= <0.01; compared with MET treated group, #P=<0.05; ns=no statistical significance.

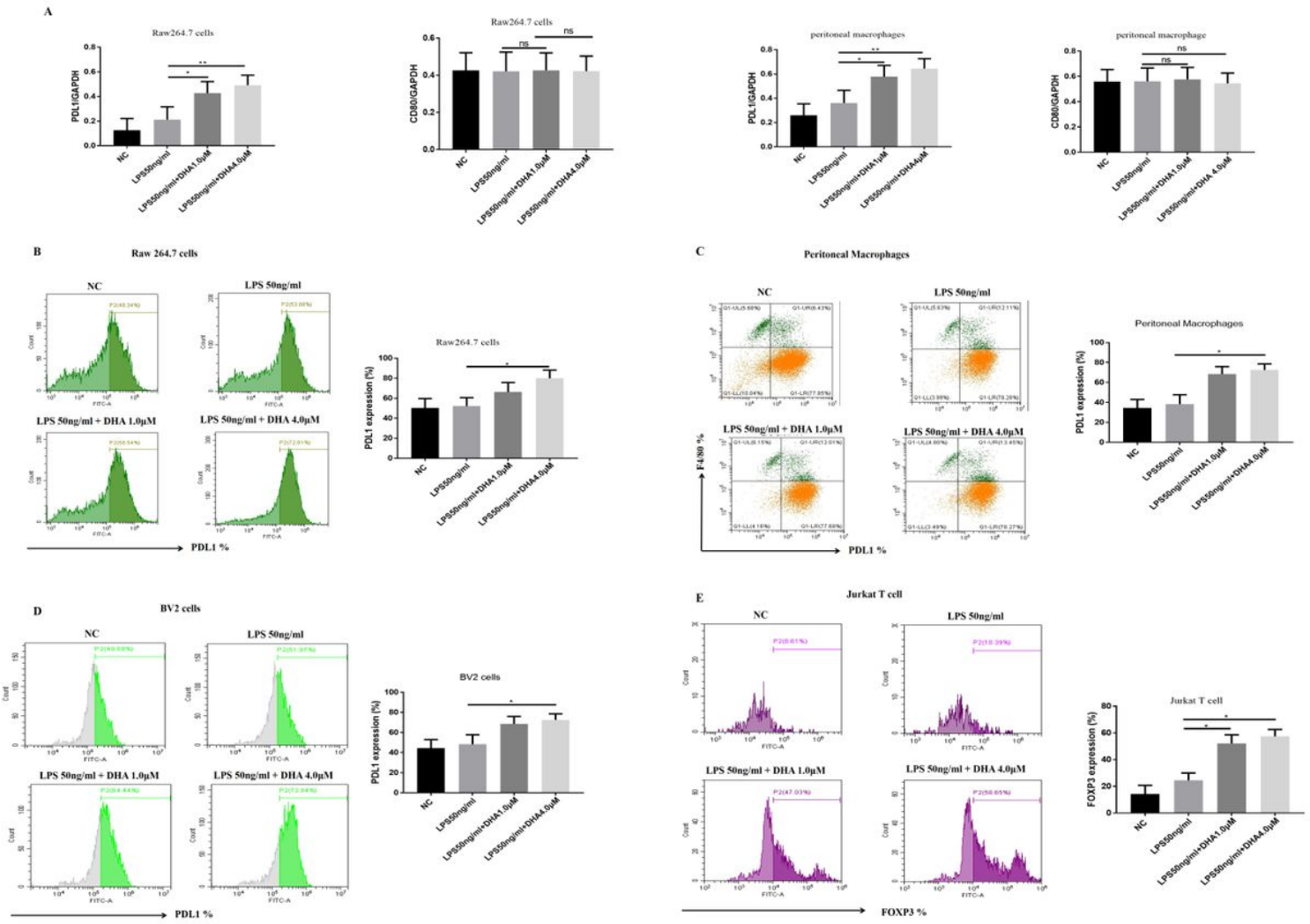

Figure 4.

Figure 4

The inflammatory –resolving effects of DHA is functionally correlated with AXL Peritoneal macrophages from C57BL/6 mice were challenged by 3% sodium thioglycolate three days in advance. A) RT-PCR analysis for PDL1 and CD80 transcription in Raw 264.7 cells and peritoneal macrophages which were treated by LPS (50ng.ml-1) and DHA (1.0/4.0μM). B, C, D) Flow cytometry assay for PDL1 expression in Raw 264.7 cells, peritoneal macrophages (PDL1+/F480+) and BV2 cells by LPS (50ng.ml-1) and DHA (1.0/4.0μM) treatment. BV2 cells were treated by DHA (1.0/4.0μM) or LPS (50ng.ml-1) for 12h, and then Jurkat T cells were co-cultured with BV2 cells for another 12h. E) FOXP3 expression on Jurkat T cells analyzed by flow cytometry. Data are representative of three independent experiments. *P=<0.05; **P= <0.01; compared with MET treated group, #P=<0.05; ns=no statistical significance.

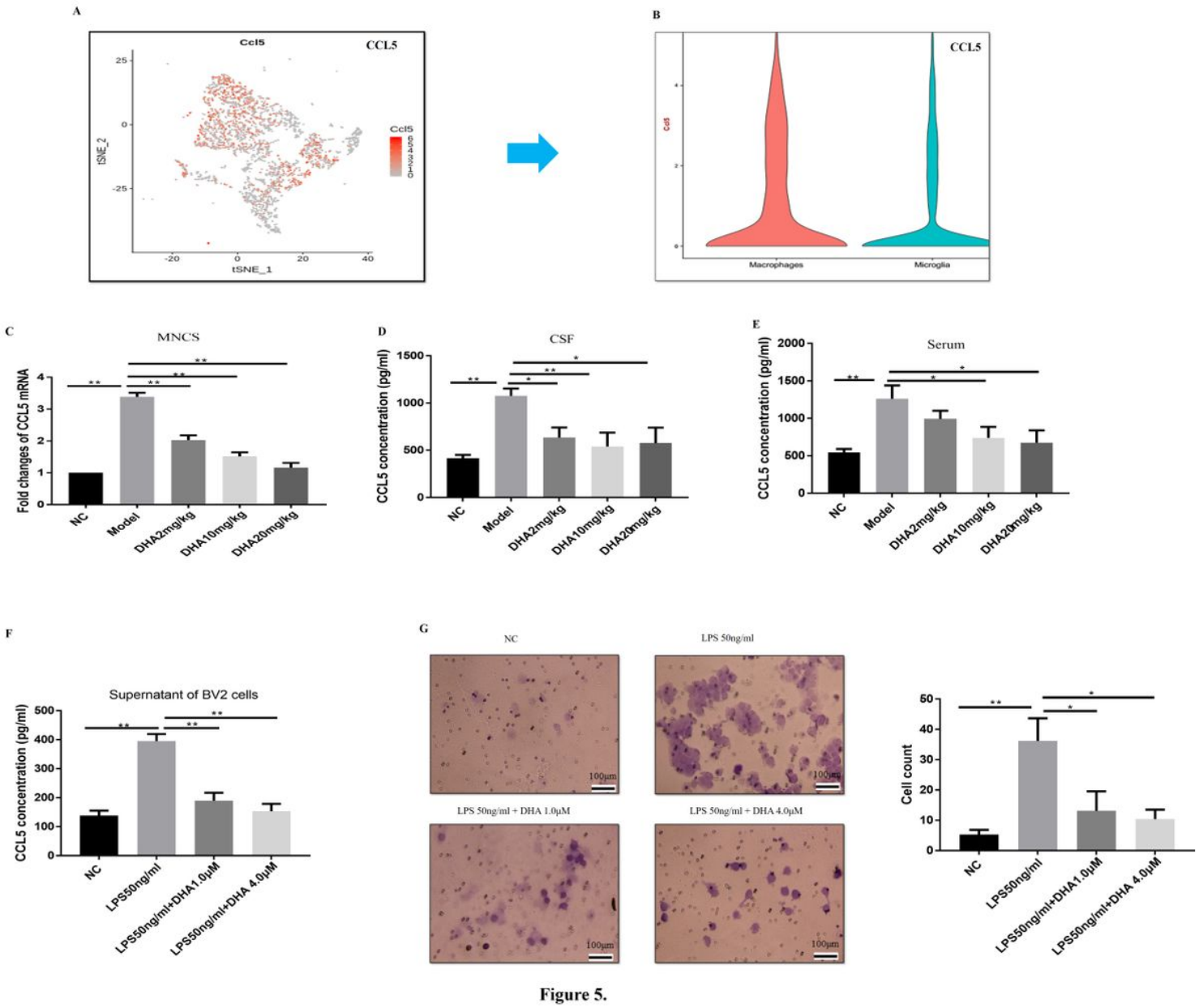

Figure 5.

Figure 5

The inflammatory –resolving effects of DHA is functionally correlated with AXL A, B) CNV analysis showed that CCL5 were almost expressed in macrophages and microglia (red, cells with detected CNVs; gray, no detected CNVs). MNCS from EAE, MET(1mg.kg-1) and DHA (2, 10, 20 mg.kg-1) mice were harvested by 30/70% percoll gradient separation. C) qRT-PCR assay for CCL5 were analyzed by LightCycler 480 Ⅱ Roche. D, E) CSF and serum were obtained from EAE, MET(1mg.kg-1) and DHA (2, 10, 20 mg.kg-1) mice, ELISA assay for CCL5 analysis were carried out by using the CSF and serum. The supernatant of BV2 cells was harvested under the treatment of DHA (1.0/4.0μM) or LPS (50ng.ml-1) for 12h, and transferred into 24-well plate for chemotaxis. F) Supernatant from BV2 cells that were treated with DHA (1.0/4.0μM) and LPS (50ng.ml-1). G) Chemotaxis ability of BV2 cells by using trans well assay. Data are representative of three independent experiments. *P=<0.05; **P=<0.01; compared with MET treated group, #P=<0.05; ns=no statistical significance.

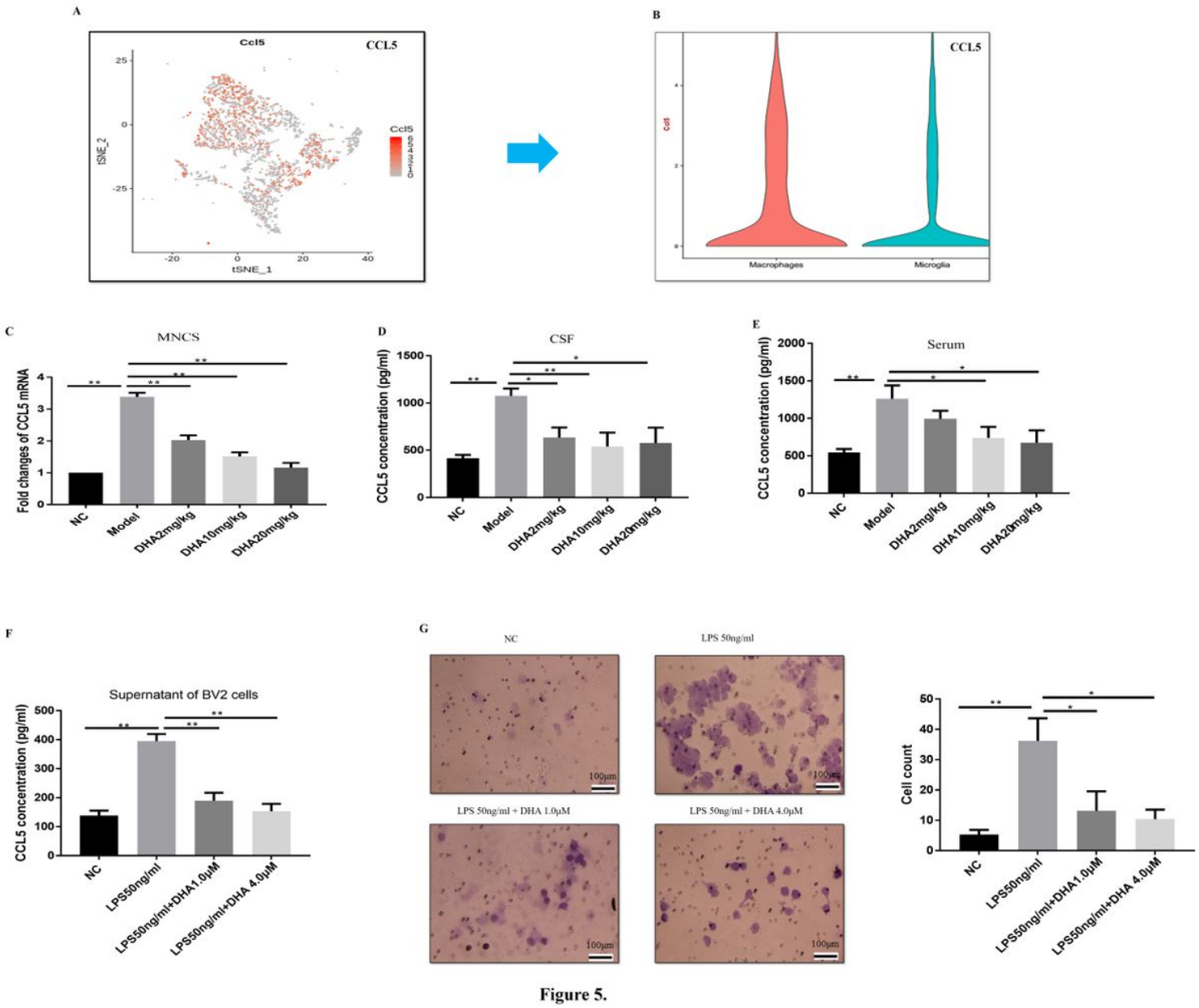

Figure 5.

Figure 5

The inflammatory –resolving effects of DHA is functionally correlated with AXL A, B) CNV analysis showed that CCL5 were almost expressed in macrophages and microglia (red, cells with detected CNVs; gray, no detected CNVs). MNCS from EAE, MET(1mg.kg-1) and DHA (2, 10, 20 mg.kg-1) mice were harvested by 30/70% percoll gradient separation. C) qRT-PCR assay for CCL5 were analyzed by LightCycler 480 Ⅱ Roche. D, E) CSF and serum were obtained from EAE, MET(1mg.kg-1) and DHA (2, 10, 20 mg.kg-1) mice, ELISA assay for CCL5 analysis were carried out by using the CSF and serum. The supernatant of BV2 cells was harvested under the treatment of DHA (1.0/4.0μM) or LPS (50ng.ml-1) for 12h, and transferred into 24-well plate for chemotaxis. F) Supernatant from BV2 cells that were treated with DHA (1.0/4.0μM) and LPS (50ng.ml-1). G) Chemotaxis ability of BV2 cells by using trans well assay. Data are representative of three independent experiments. *P=<0.05; **P=<0.01; compared with MET treated group, #P=<0.05; ns=no statistical significance.

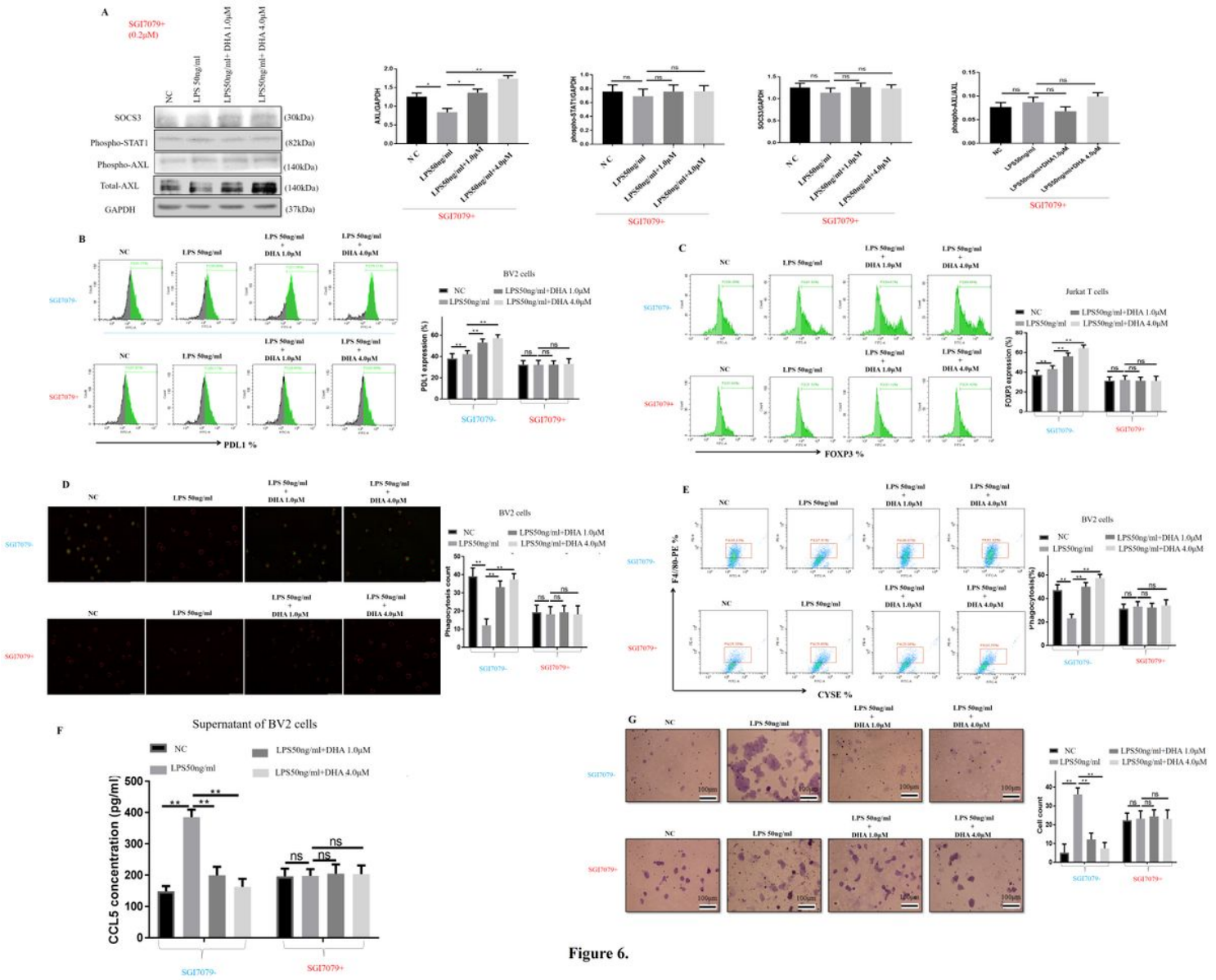

Figure 6

The inflammatory-resolving effects of DHA necessitated the AXL signaling in microglia BV2 cells treated by SGI7079 (0.2μM), DHA (1.0/4.0μM) or LPS (50 ng.ml-1) for 12h, and then Jurkat T cells were co-cultured with BV2 cells for another 12h. A) BV2 cells were then analyzed for Phospho-STAT1; SOCS3; phospho-AXL and Total-AXL by western blot. B, C) Flow cytometry showed PDL1 expression on and FOXP3 expression on Jurkat T cells. PC12 cells were induced by apoptosis by 5-F and then transferred into BV2 cells for 2h. D, E) Fluorescence microscope images (400×) showed count of phagocytosis cell by BV2 cells and Flow cytometry assay showed the percent of phagocyting apoptosis cell (CYSE+/F480+) under the treatment of SGI7079 (0.2μM), DHA (1.0/4.0μM) or LPS(50ng.ml-1). The supernatant of BV2 cells was harvested under the treatment of SGI7079 (0.2μM), DHA (1.0/4.0μM) or LPS (50ng.ml-1) for 12h, and transferred into 24-well plate for chemotaxis. F, G) ELISA assay and trans-well assay showed the influence of CCL5 expression treated by SGI7079. Data are representative of three independent

experiments. *P=<0.05; **P=<0.01; compared with MET treated group, #P=<0.05; ns=no statistical significance.

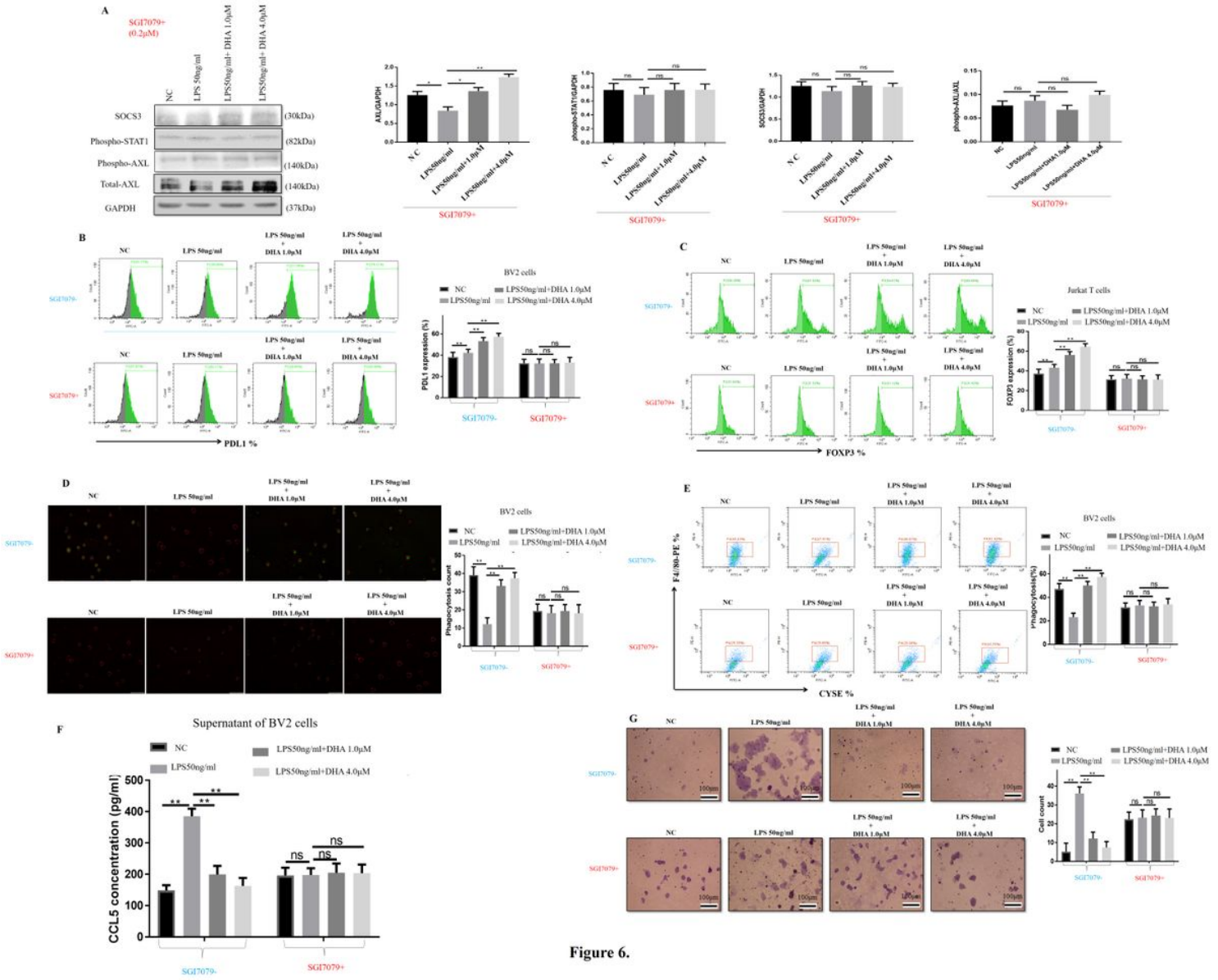

Figure 6.

Figure 6

The inflammatory-resolving effects of DHA necessitated the AXL signaling in microglia BV2 cells treated by SGI7079 (0.2μM), DHA (1.0/4.0μM) or LPS (50 ng.ml-1) for 12h, and then Jurkat T cells were co-cultured with BV2 cells for another 12h. A) BV2 cells were then analyzed for Phospho-STAT1; SOCS3; phospho-AXL and Total-AXL by western blot. B, C) Flow cytometry showed PDL1 expression on and FOXP3 expression on Jurkat T cells. PC12 cells were induced by apoptosis by 5-F and then transferred into BV2 cells for 2h. D, E) Fluorescence microscope images (400×) showed count of phagocytosis cell by BV2 cells and Flow cytometry assay showed the percent of phagocyting apoptosis cell (CYSE+/F480+) under the treatment of SGI7079 (0.2μM), DHA (1.0/4.0μM) or LPS(50ng.ml-1). The supernatant of BV2 cells was harvested under the treatment of SGI7079 (0.2μM), DHA (1.0/4.0μM) or LPS (50ng.ml-1) for 12h, and transferred into 24-well plate for chemotaxis. F, G) ELISA assay and trans-well assay showed the

influence of CCL5 expression treated by SGI7079. Data are representative of three independent experiments. *P=<0.05; **P=<0.01; compared with MET treated group, #P=<0.05; ns=no statistical significance.

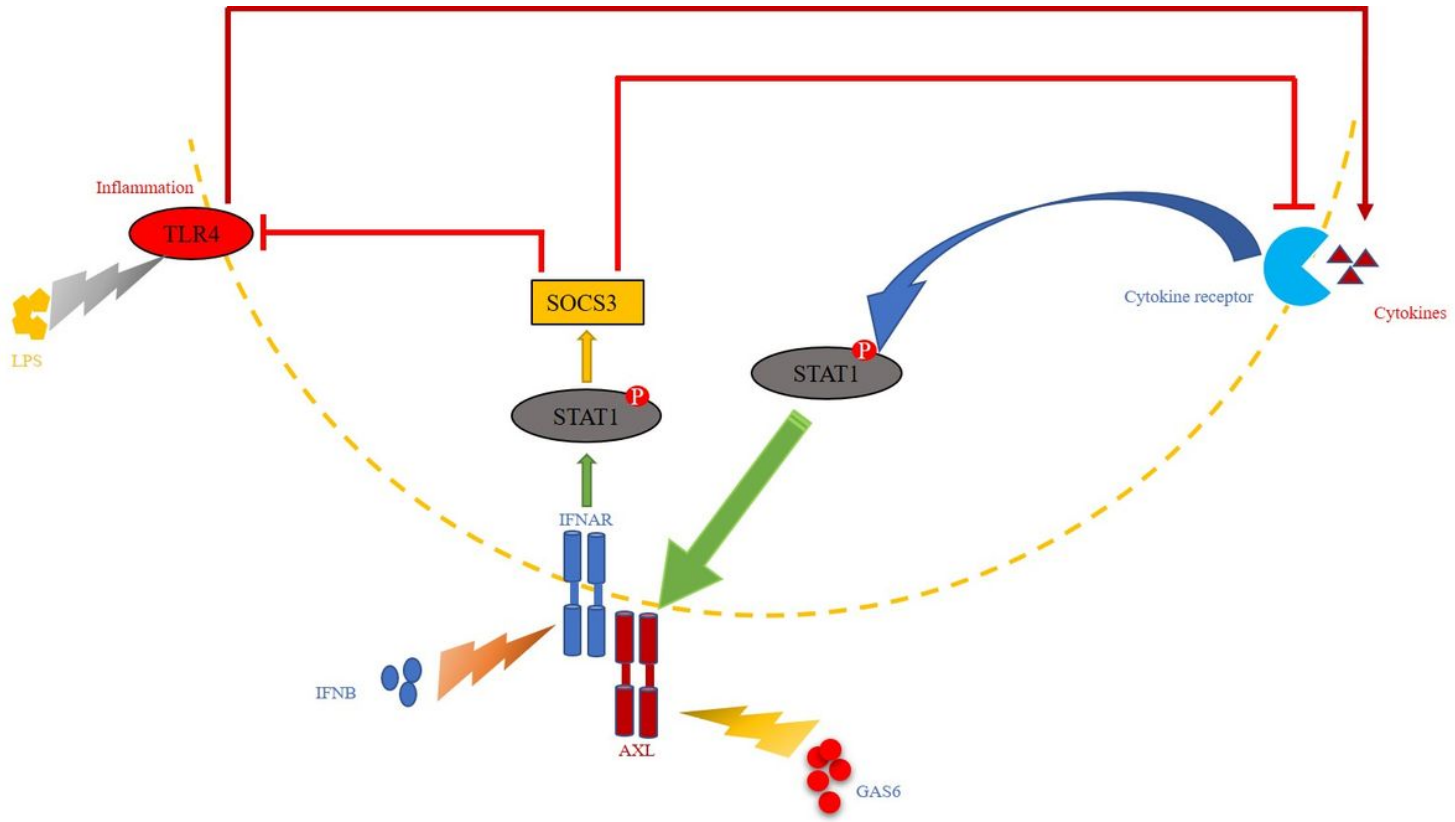

Figure 7.

Figure 7

Large amounts of researchers have found that, specifically under the pro-inflammatory conditions, AXL interacted with type I interferon receptor (IFNAR) and potentiated the downstream inflammatory-resolving events as represented by the activation of STAT1:SOCS3 pathway. Of great interest, as the molecular switch for inflammation from promotion to resolution, the transcription of AXL itself is inversely facilitated by STAT1, a central inflammatory sensor regulated by various types of pro-inflammatory signals including IFN-β ligation to IFNAR. This forms the endogenous basis for the negative feedback loop of immune responses and consequently maintains the homeostasis in inflammatory microenvironment (graphically shown in below, Figure 7.).

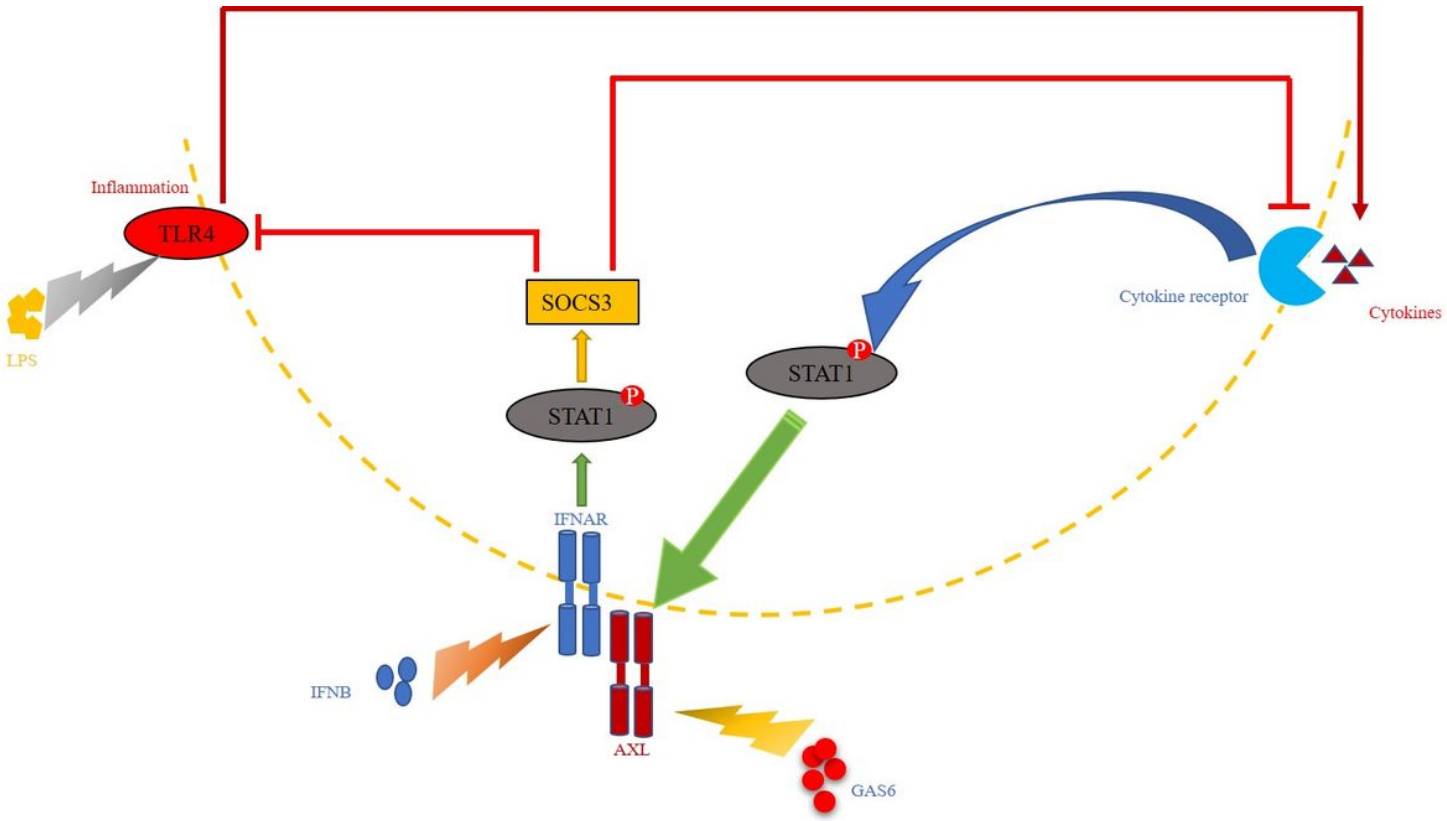

Figure 7.

Figure 7

Large amounts of researchers have found that, specifically under the pro-inflammatory conditions, AXL interacted with type I interferon receptor (IFNAR) and potentiated the downstream inflammatory-resolving events as represented by the activation of STAT1:SOCS3 pathway. Of great interest, as the molecular switch for inflammation from promotion to resolution, the transcription of AXL itself is inversely facilitated by STAT1, a central inflammatory sensor regulated by various types of pro-inflammatory signals including IFN-β ligation to IFNAR. This forms the endogenous basis for the negative feedback loop of immune responses and consequently maintains the homeostasis in inflammatory microenvironment (graphically shown in below, Figure 7.).

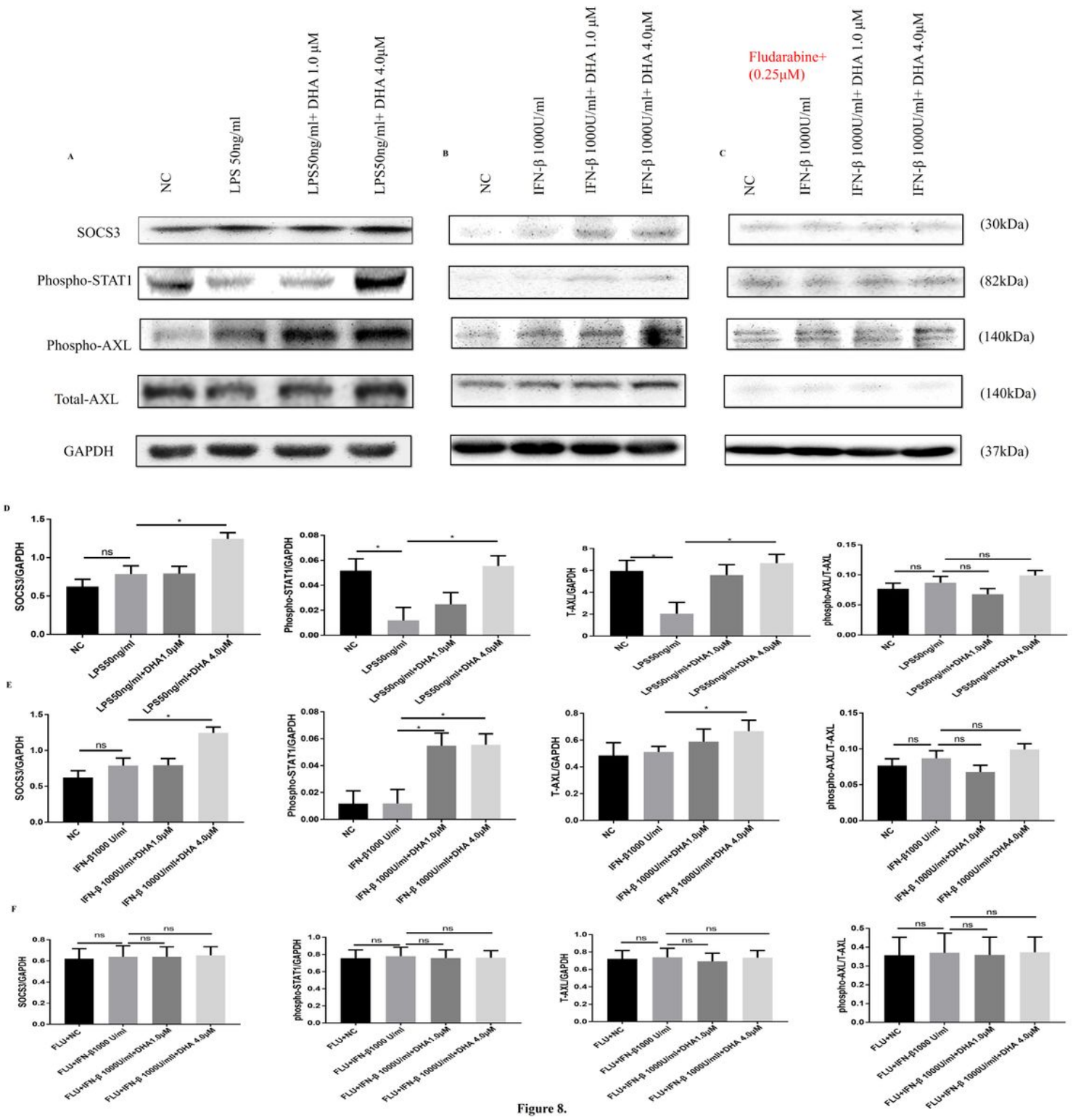

Figure 8.

Figure 8

DHA specifically rebalanced overactivated inflammation by regulating AXL related STAT1:SOCS3 pathway A, D) BV2 cells treated by DHA (1.0/4.0μM) or LPS(50 ng.ml-1) for 12h. Cells were then analyzed for Phospho-STAT1; SOCS3; phospho-AXL and Total-AXL by Western blot. B, C, E, F) BV2 cells were treated by DHA(1.0/4.0μM) for 24h, Fludarabine(0.25μM) for, or IFN- β (1000U.ml-1) for 12h. Cells were then analyzed for Phospho-STAT1; SOCS3; phospho-AXL and Total-AXL by Western blot. Data are

representative of three independent experiments. *P=<0.05; **P=<0.01; compared with MET treated group, #P=<0.05; ns=no statistical significance.

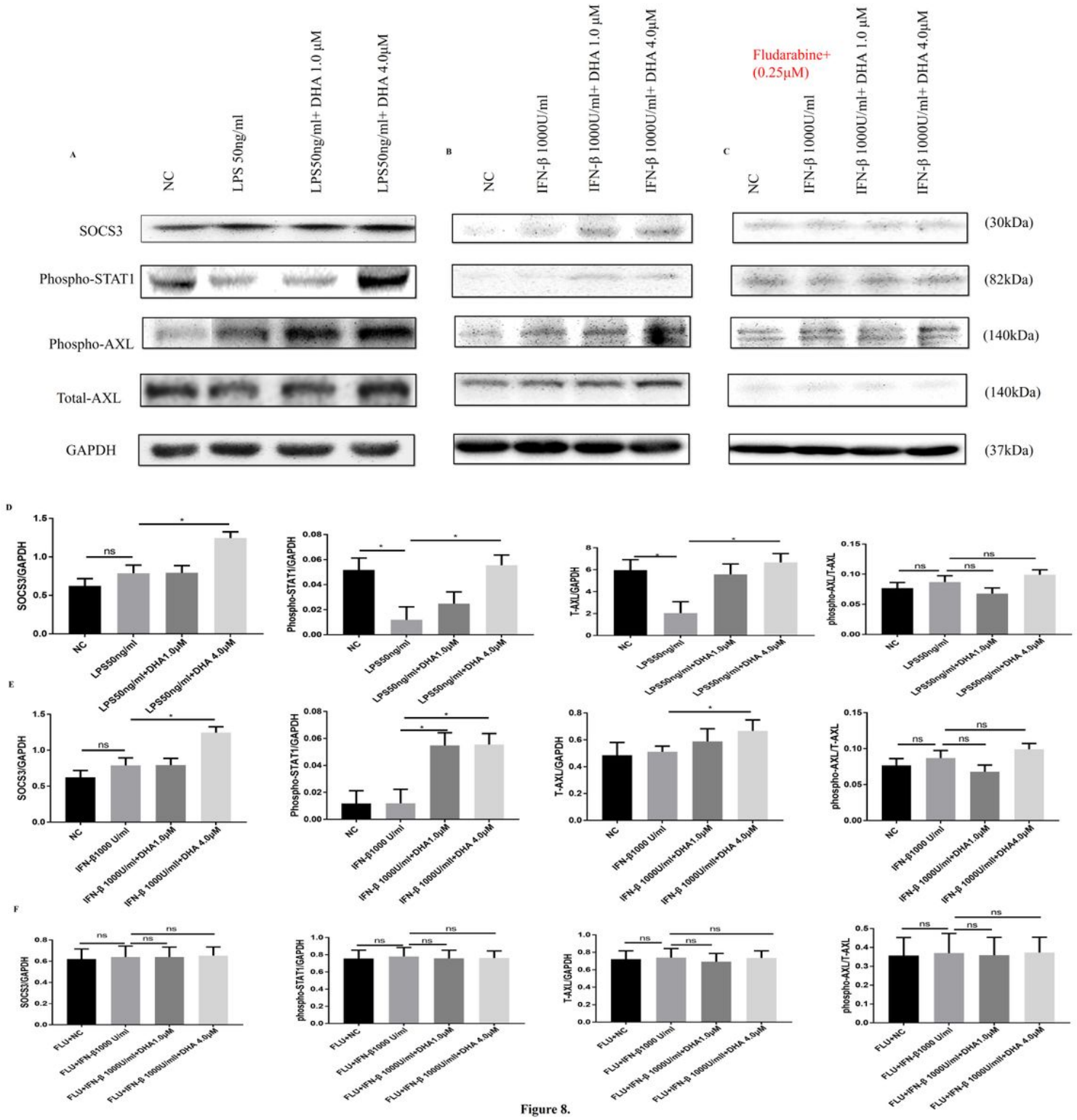

Figure 8.

Figure 8

DHA specifically rebalanced overactivated inflammation by regulating AXL related STAT1:SOCS3 pathway A, D) BV2 cells treated by DHA (1.0/4.0μM) or LPS(50 ng.ml-1) for 12h. Cells were then analyzed for Phospho-STAT1; SOCS3; phospho-AXL and Total-AXL by Western blot. B, C, E, F) BV2 cells were

treated by DHA(1.0/4.0μM) for 24h, Fludarabine(0.25μM) for, or IFN- β (1000U.ml-1) for 12h. Cells were then analyzed for Phospho-STAT1; SOCS3; phospho-AXL and Total-AXL by Western blot. Data are representative of three independent experiments. *P=<0.05; **P=<0.01; compared with MET treated group, #P=<0.05; ns=no statistical significance.

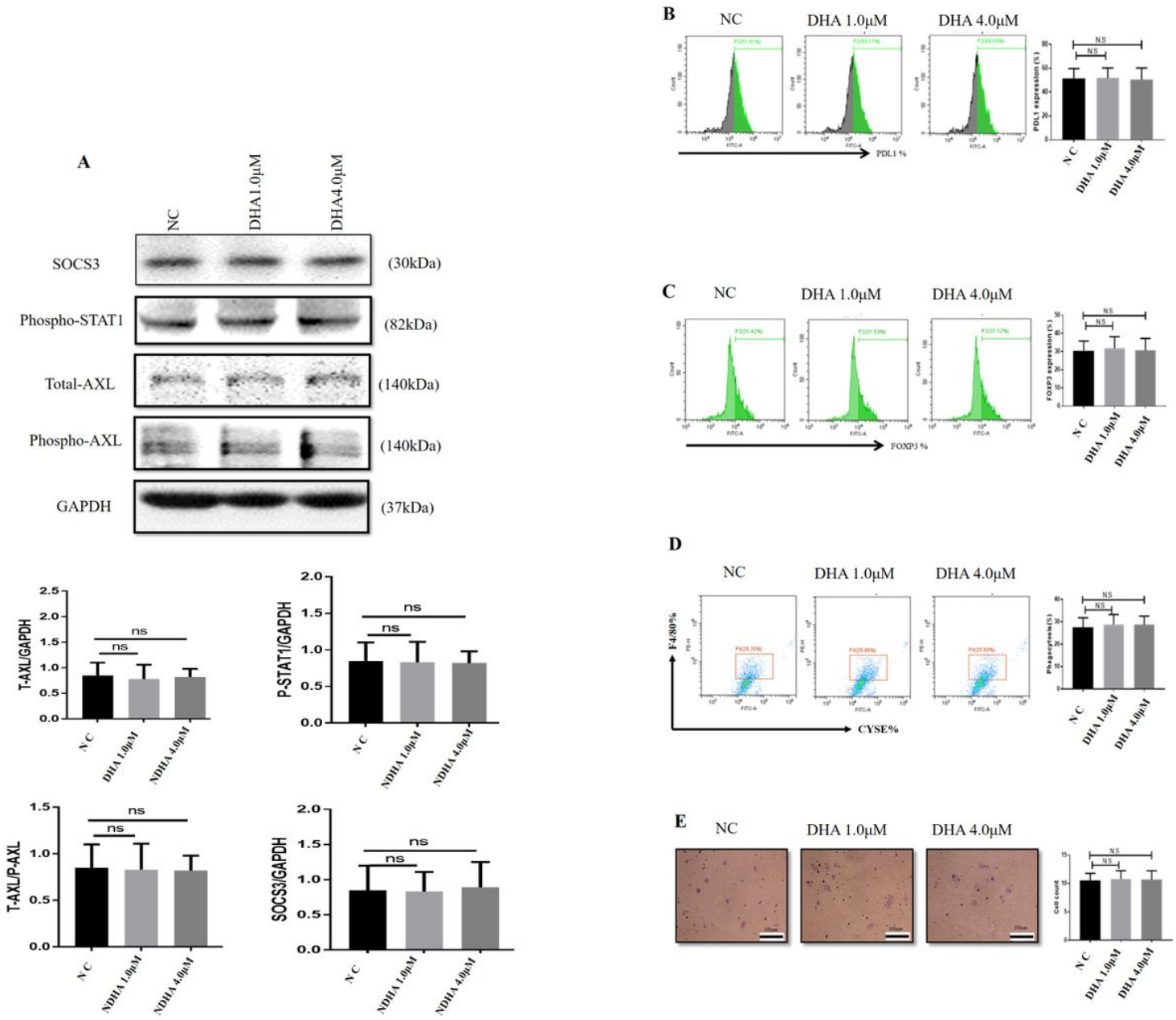

Figure 9.

Figure 9

DHA specifically rebalanced overactivated inflammation by regulating AXL related STAT1:SOCS3 pathway A) BV2 cells treated by DHA (1.0/4.0μM) for 24h. Cells were then analyzed for Phospho-STAT1; SOCS3; phospho-AXL and Total-AXL by Western blot. B, C, D, E) The regulatory effects of DHA on antigen presentation, T cell regulation, chemotactic sensitivity and phagocytic potential. Data are representative

of three independent experiments. *P=<0.05; **P=<0.01; compared with MET treated group, #P=<0.05; ns=no statistical significance.

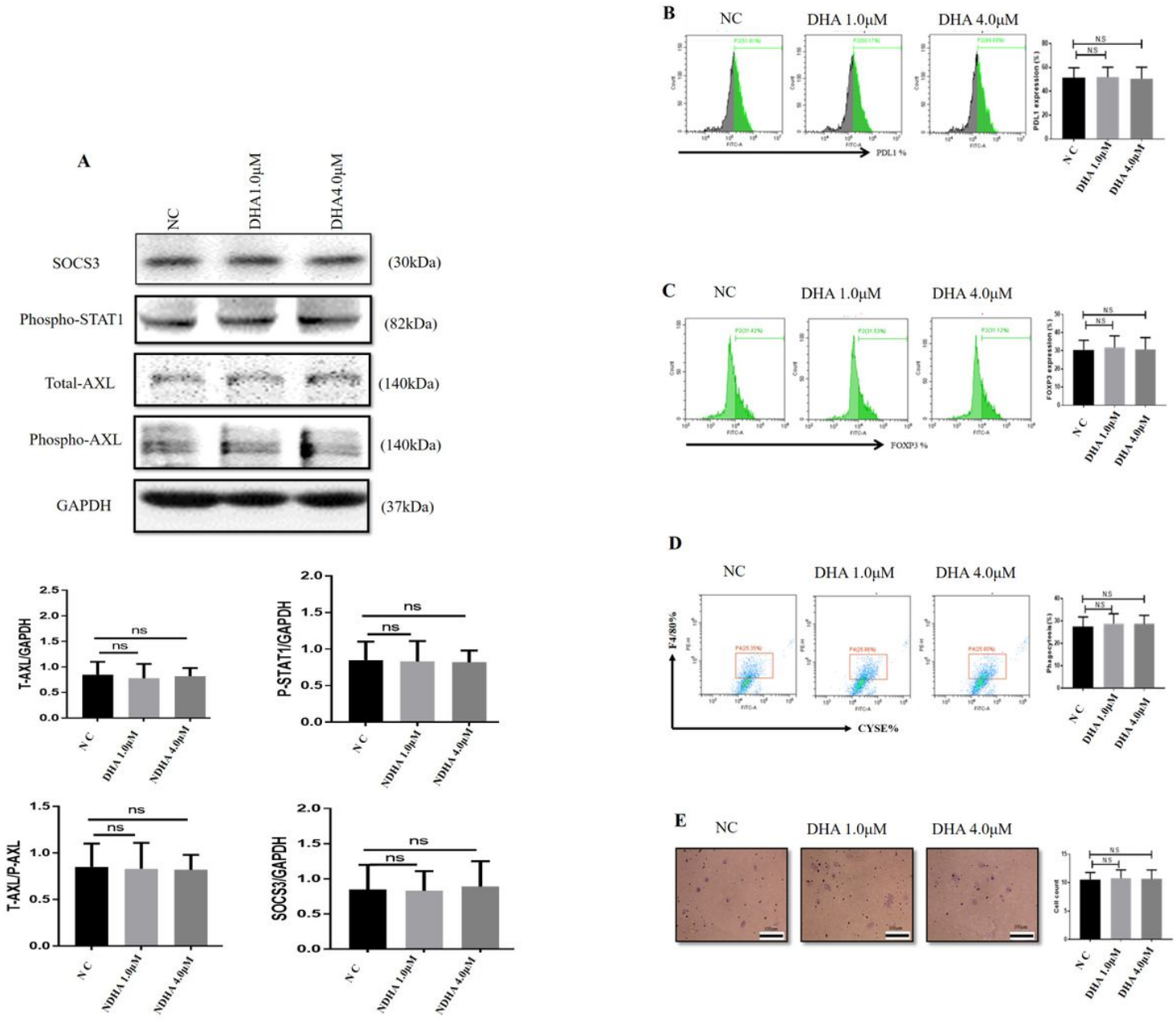

Figure 9.

Figure 9

DHA specifically rebalanced overactivated inflammation by regulating AXL related STAT1:SOCS3 pathway A) BV2 cells treated by DHA (1.0/4.0μM) for 24h. Cells were then analyzed for Phospho-STAT1; SOCS3; phospho-AXL and Total-AXL by Western blot. B, C, D, E) The regulatory effects of DHA on antigen presentation, T cell regulation, chemotactic sensitivity and phagocytic potential. Data are representative of three independent experiments. *P=<0.05; **P=<0.01; compared with MET treated group, #P=<0.05; ns=no statistical significance.

Supplementary Files

This is a list of supplementary files associated with this preprint. Click to download.

- graphicalabstarct.png
- graphicalabstarct.png